Three-dimensional mixed-wet random pore-scale network modeling of two- and three-phase flow in porous media. I. Model description

Mohammad Piri* and Martin J. Blunt
Department of Earth Science and Engineering, Imperial College, London SW7 2AZ, United Kingdom
(Received 26 January 2004; published 4 February 2005)

We present a three-dimensional network model to simulate two- and three-phase capillary dominated processes at the pore level. The displacement mechanisms incorporated in the model are based on the physics of multiphase flow observed in micromodel experiments. All the important features of immiscible fluid flow at the pore scale, such as wetting layers, spreading layers of the intermediate-wet phase, hysteresis, and wettability alteration are implemented in the model. Wettability alteration allows any values for the advancing and receding oil-water, gas-water, and gas-oil contact angles to be assigned. Multiple phases can be present in each pore or throat (element), in wetting and spreading layers, as well as occupying the center of the pore space. In all, some 30 different generic fluid configurations for two- and three-phase flow are analyzed. Double displacement and layer formation are implemented as well as direct two-phase displacement and layer collapse events. Every element has a circular, square, or triangular cross section. A random network that represents the pore space in Berea sandstone is used in this study. The model computes relative permeabilities, saturation paths, and capillary pressures for any displacement sequence. A methodology to track a given three-phase saturation path is presented that enables us to compare predicted and measured relative permeabilities on a point-by-point basis. A robust displacement-based clustering algorithm is also presented.

DOI: 10.1103/PhysRevE.71.026301 PACS number(s): 47.55.Mh, 68.08.Bc

I. INTRODUCTION

The simultaneous flow of three phases—oil, water, and gas—in porous media is of great interest in many areas of science and technology, such as petroleum reservoir and environmental engineering. Three fluid flow occurs in enhanced oil recovery schemes including tertiary gas injection into oil and water, gas cap expansion, solution gas drive, gravity drainage, water flooding with different initial oil and gas saturations, steam injection, thermal flooding, depressurization below the bubble point, and water alternate gas (WAG) injection. In an environmental context three-phase flow occurs when a nonaqueous phase liquid (NAPL), leaking from an underground storage tank for instance, migrates through the unsaturated zone and may coexist with water and air (gaseous phase).

In order to understand fluid flow in porous media, one needs to know the constitutive relationships between macroscopic properties of the system such as relative permeabilities, capillary pressures, and fluid saturations. These relationships are used in macroscopic partial differential equations to describe the transport of fluid. The determination of constitutive relationships is complicated as they are dependent on the fluids' properties, the pore space, and the saturation history.

Experimental measurements of three-phase relative permeabilities and capillary pressures are extremely difficult to perform and at low saturation the results are very uncertain [1–4]. Two independent fluid saturations are required to define a three-phase system and there is an infinite number of possible fluid arrangements making a comprehensive suite of experimental measurements for all three-phase displacements impossible. This is why numerical simulations of three-phase flow almost always rely on available empirical correlations to predict relative permeability and capillary pressure from measured two-phase properties [5–26]. These models may give predictions that vary as much as an order of magnitude from each other, or from direct measurements, since they have little or no physical basis [14,25,27].

It is important to have a reliable physically based tool that can provide plausible estimates of macroscopic properties. Any theoretical or numerical approach to this problem not only needs a *detailed understanding* of the multiphase displacement mechanisms at the pore level but also an accurate and realistic characterization of the *structure* of the porous medium [28]. During the last two decades our knowledge of the physics of two- and three-phase flow at the pore level has considerably increased through experimental investigation of displacements in core samples and micromodels [29–43]. To describe the geometry of the pore space several authors have developed different statistical [44–46] and process based [47–49] techniques. In addition the pore space can be imaged directly using micro-CT tomography [50,51]. An example of a three-dimensional pore space image of a sandstone is shown in Fig. 1. It is possible to simulate multiphase flow directly on a three-dimensional pore-space image by solving Navier-Stokes equations or by using Lattice-Boltzman techniques [52–55]. However, for capillary-controlled flow with multiple phases, these methods become cumbersome and computationally expensive.

An attractive alternative approach is to describe the pore space as a network of pores connected by throats with some idealized geometry (see Fig. 2) [49,56]. Then a series of

*Present address: Department of Civil and Environmental Engineering, Engineering Quad E-228, Princeton University, Princeton, New Jersey 08544, USA. Electronic address: mpiri@princeton.edu

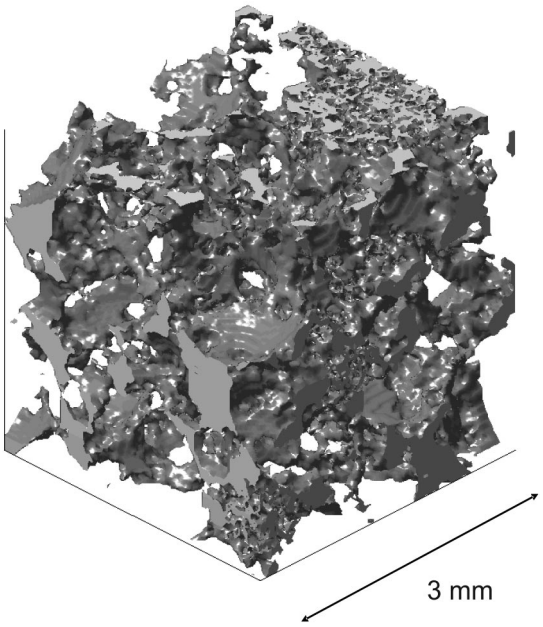

FIG. 1. The void space of a sandstone produced by process based simulation [47–49].

displacement steps in each pore or throat are combined to simulate multiphase flow. Fatt [57–59] initiated this approach by using a regular two-dimensional network to find capillary pressure and relative permeability. Since then, the capabilities of network models have improved enormously and have been applied to describe many different processes. Recent advances in pore-scale modeling have been reviewed by Celia *et al.* [60], Blunt [61], and Blunt *et al.* [62].

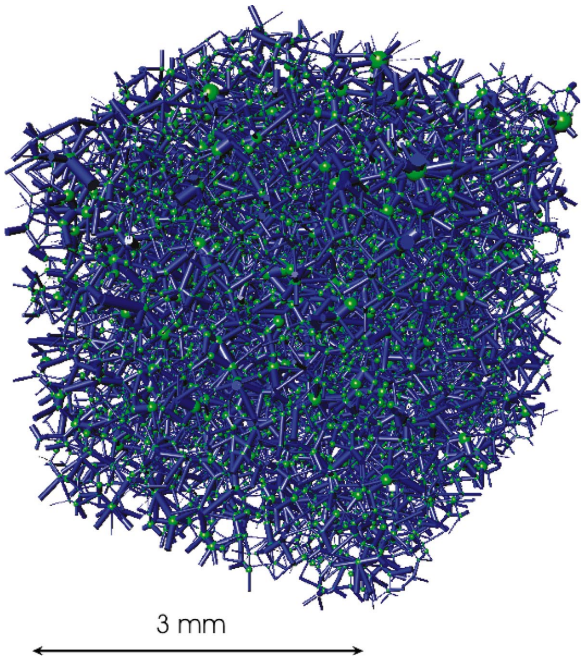

FIG. 2. (Color) The Berea network used in this paper. The network is a disordered lattice of pores connected by throats. The network topology, the radii of the pores and throats, their shapes, and their volumes are all determined from a three-dimensional representation of the pore space of the system of interest (see Fig. 1). This network will be used to predict two- and three-phase relative permeabilities (see Table II for dimensions and statistics of the network).

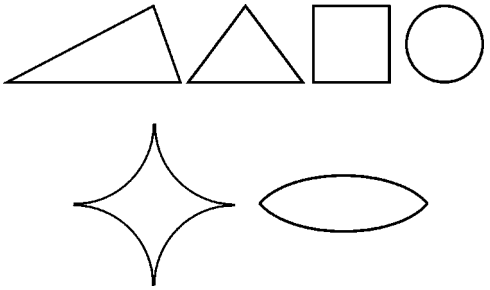

FIG. 3. Elements with different cross-sectional shape.

For a random close packing of spheres Bryant and coworkers were able to predict permeability, elastic, and electrical properties and relative permeability [63–65]. Øren *et al.* extended this approach by reconstructing a variety of sandstones and generating topologically equivalent networks from them. Using these networks several authors have been able to predict relative permeability and oil recovery for a variety of systems [47–49,66–70].

In this paper we extend this predictive approach to three-phase flow. Before reviewing previous three-phase network models, we review the fundamentals of contact angles, spreading coefficient, wettability alteration, and spreading and wetting layers as well as describing the network we use.

II. POROUS MEDIUM

In recent years, several advances have been made in the construction of realistic representations of porous media. Øren, Bakke, and co-workers [47–49] have developed random network models based on the pore space geometry of the rock of interest. The model is derived either from a direct three-dimensional image of the pore space obtained from micro-CT scanning, or from simulating the geological processes by which the rock was formed, see Fig. 1. Many other authors have also developed techniques to derive pore structures from a variety of measurements [46,51,63–65,71–83]. While such approaches are not routine, and the correct pore space characterization of carbonates is very much an open question, for simple sandstones there are reliable methods for determining an equivalent network structure that attempts to mimic the properties of the real pore space.

In cross section, individual pores and throats are often modeled as triangles and high-order polygons [84,85]. This allows wetting phase to occupy the corners when the nonwetting phase fills the center. As well as triangular cross section elements, authors have used geometries with circular [86,87], square [88–90], star-shape [91,92], and lenticular [28] cross sections (see Fig. 3) to represent pores and throats.

The network model in this work reads as input any two or three-dimensional regular or random network comprised of pores connected by throats. Each pore or throat is assigned a total volume, an inscribed radius, and a cross-sectional shape. In this model the pore and throats have a scalene

TABLE I. Network parameters read by the model consistent with the networks generated by Øren, Bakke, and co-workers [47–49].

No.	Item	No.	Item
1	total number of pores and throats	11	shape factor of each pore and throat
2	length, width, and depth of the network	12	clay pore volume
3	volume of each pore and throat	13	index of the first and second connecting pores to each throat
4	*X*, *Y*, and *Z* coordinations of each pore	14	microporosity volume in each throat
5	inscribed radius of each pore and throat	15	spacing[a]
6	number of connecting pore(s) to each pore[b]	16	length of the first and second pore connecting to each throat
9	index of connecting pore(s) to each pore	17	length of each throat
8	whether each pore is at the inlet		
9	whether each pore is at the outlet		
10	index of the throat connecting two pores		

[a]Distance between the centers of the two connecting pores.
[b]Coordination number of each pore.

triangular, square, or circular cross section. The cross section has the same shape factor G (ratio of cross-sectional area A to perimeter P, squared) [85] as the real system from which the network is derived,

$$G = \frac{A}{P^2}. \tag{1}$$

A clay volume is associated with the network. This represents an immobile volume that remains water saturated throughout all displacements. It can be adjusted to match the observed connate water saturation [47–49]. Table I lists all the parameters that the model reads to recognize a network.

A Berea network is used for the modeling studies in this work. A network of pores and throats is generated that presents the topology of the void space of the rock of interest (see Fig. 2). The pores and throats have sizes and shapes that reproduce the principal geometric features of the three-dimensional image (see Fig. 2) [48]. Table II lists the network statistics. Figure 4 compares the pore and throat size distributions of the network.

III. PHYSICS OF THREE-PHASE FLOW AT THE PORE LEVEL

A. Spreading coefficients and interfacial tensions

The ability of oil to spread on water in the presence of gas is described by the *spreading coefficient* which is a representation of the force balance where the three phases meet. If the interfacial tensions are found by contacting pairs of pure fluids in the absence of the third, the coefficient is called *initial* and is defined by [93]

$$C_s^i = \sigma_{gw} - \sigma_{go} - \sigma_{ow}, \tag{2}$$

where σ is an interfacial tension between two phases labeled o, w, and g to stand for oil, water, and gas, respectively. However, when three phases are present simultaneously, the interfacial tensions are different from those in two-phase systems. For instance, the gas/water interfacial tension may be significantly lower than its two-phase value because oil may cover the interface by a thin film of molecular thickness [94]. The other two-phase interfacial tensions may also vary when

TABLE II. Berea network statistics.

Item	Throats	Pores	Total
Number	26146	12349	38495
Porosity excl. clay (%)	4.562	13.746	18.309
Porosity incl. clay (%)	6.238	17.785	24.024
Average shape factor	0.035	0.033	0.034
Triangular cross sections (%)	90.729	95.506	92.261
Square cross sections (%)	7.542	4.324	6.510
Circular cross sections (%)	1.729	0.170	1.229
ASCHA (deg)[a]	15.235	13.744	14.751
AWCHA (deg)[b]	48.828	49.215	48.954
Minimum radius (μm)	0.903	3.623	0.903
Maximum radius (μm)	56.850	73.539	73.539
Average radius (μm)	10.970	19.167	13.60
Connected to the inlet	254	0	254
Connected to the outlet	267	0	267
Isolated clusters			3
Isolated	3	6	9
Minimum coordination number		1	
Maximum coordination number		19	
Average coordination number		4.192	
Clay volume (%)	1.676	4.039	5.715
K_{abs} (cal. box: 0.05–0.95) (mD)			3055
X dimension (mm)			3
Y dimension (mm)			3
Z dimension (mm)			3

[a]Average sharpest corner half angle.
[b]Average widest corner half angle.

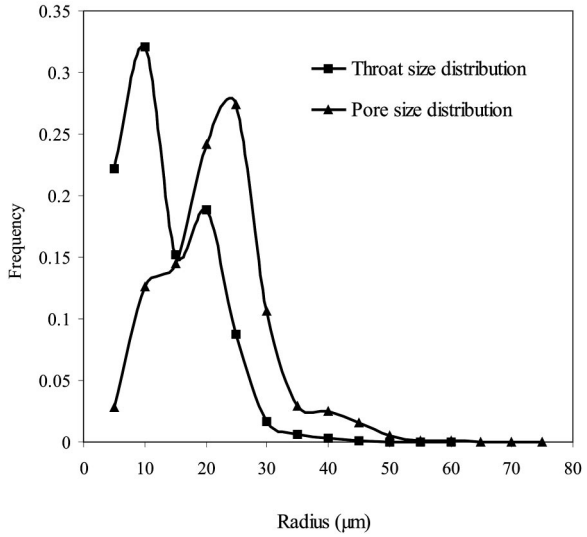

FIG. 4. Pore and throat size distributions for the Berea network.

the third phase is present. If the three phases remain long enough in contact, thermodynamic equilibrium will be reached when liquids become mutually saturated. In these circumstances the spreading coefficient is named *equilibrium* and is given by Eq. (3), which is either negative or zero [93],

$$C_s^{eq} = \sigma_{gw}^{eq} - \sigma_{go}^{eq} - \sigma_{ow}^{eq}. \tag{3}$$

Three-phase systems may be divided into one of the following cases: (a) *Nonspreading*, $C_s^i < 0$: a blob of oil will remain stationary on water; for example, CS_2 on water [93]. (b) *Partially spreading*, $C_s^i > 0$ and $C_s^{eq} < 0$: where a quick initial spreading happens and then when the water surface is covered by a thin oil film, oil retracts to a lens. An example is benzene on water. (c) *Spreading*, $C_s^i > 0$ and $C_s^{eq} \approx 0$: in this case, oil spreads on water and excess oil makes the film thicker and thicker. When the thickness of the oil film is larger than the range of intermolecular forces the equilibrium spreading coefficient becomes zero. Soltrol, a mixture of hydrocarbons, is an example of this case [42].

B. Three-phase contact angles

The contact angle is defined as the angle between the two-phase line and the solid surface measured through the denser phase. In a three phase system a horizontal force balance can be written for each of the three pairs of fluids, i.e., oil-water, gas-water, and gas-oil, residing on a solid (see Fig. 5):

$$\sigma_{os} = \sigma_{ws} + \sigma_{ow} \cos \theta_{ow}, \tag{4}$$

$$\sigma_{gs} = \sigma_{ws} + \sigma_{gw} \cos \theta_{gw}, \tag{5}$$

$$\sigma_{gs} = \sigma_{os} + \sigma_{go} \cos \theta_{go}. \tag{6}$$

A constraint between the three-phase contact angles and interfacial tensions in mutual equilibrium can be derived by manipulation of Eqs. (4)–(6):

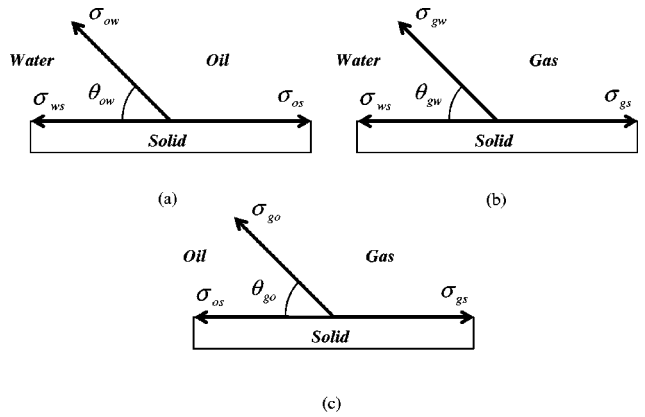

FIG. 5. Horizontal force balance in three two-phase systems: (a) oil-water-solid, (b) gas-water-solid, and (c) gas-oil-solid.

$$\sigma_{gw}^{eq} \cos \theta_{gw} = \sigma_{go}^{eq} \cos \theta_{go} + \sigma_{ow}^{eq} \cos \theta_{ow}. \tag{7}$$

Equation (7) was derived by Bartell and Osterhoff [95] in the context of solid-oil-water systems and then by Zhou and Blunt [94] in contaminant hydrology. This constraint has many implications for three-phase processes. For instance, consider a three-phase strongly oil-wet system, i.e., $\theta_{ow} \approx 180°$. At ambient conditions, typical interfacial tensions for water/*n*-alkane systems are $\sigma_{go}^{eq} = 20$ mN/m and $\sigma_{ow}^{eq} = 50$ mN/m [93]. This means $\sigma_{gw}^{eq} \cos \theta_{gw} < 0$ which in turn implies $\theta_{gw} > 90°$. The analysis above for oil-wet systems indicates that gas is not the most nonwetting phase in the presence of water.

In the rest of the paper we will drop the superscript *eq* and always assume that we are dealing with interfacial tensions at equilibrium.

Blunt [96] showed in a n phase system there are $n(n-1)/2$ contact angles, $(n-1)(n-2)/2$ constraints, and $(n-1)$ independent contact angles. In three-phase systems, only two of the contact angles need to be defined independently.

Van Dijke *et al.* [97] presented a linear relationship to find gas-oil and gas-water contact angles from the oil-water contact angle and interfacial tensions which also satisfy the constraint given by Eq. (7):

$$\cos \theta_{go} = \frac{1}{2\sigma_{go}} \{C_s \cos \theta_{ow} + C_s + 2\sigma_{go}\}, \tag{8}$$

$$\cos \theta_{gw} = \frac{1}{2\sigma_{gw}} \{(C_s + 2\sigma_{ow}) \cos \theta_{ow} + C_s + 2\sigma_{go}\}. \tag{9}$$

C. Wettability alteration and contact angle hysteresis

While most clean rock surfaces in contact with refined oils are water-wet, few, if any, oil reservoirs are completely water-wet. This is because of direct contact of crude oil with the solid surface which changes its wettability by adsorption of the polar components of the crude or the presence of naturally oil-wet minerals within the rock. This makes any values of oil-water and consequently gas-water and gas-oil contact

angles possible [98–102]. Kovscek *et al.* [100] developed a model where the wettability of the rock surface is assumed to be altered by the direct contact of oil. Before a porous medium is invaded by oil it is assumed to be full of water and water-wet. Once it is invaded by oil a thin film of water prevents oil touching the solid surface directly. But at a threshold capillary pressure this film can collapse and allows oil to contact the solid surface and change its wettability. Regions of the pore space not contacted by oil remain water-wet.

The contact angle also depends on the direction of displacement. This difference between *advancing*, i.e., the wetting phase displacing the nonwetting one, and *receding*, i.e., nonwetting phase displacing the wetting one, contact angles may be as large as 50°–90° [93,103,104] depending on surface roughness, surface heterogeneity, swelling, rearrangement, or alteration of the surface by solvent [93].

To accommodate any type of displacement process, we assign eight contact angles to each pore and throat: θ_{ow}^{PD} (oil displacing water in an element that has not changed its wettability before), θ_{gw}^{PD} (gas displacing water in an element that has not changed its wettability before), and six contact angles when the wettability has been altered: θ_{ow}^{a} (water displacing oil), θ_{ow}^{r} (oil displacing water), θ_{gw}^{a} (water displacing gas), θ_{gw}^{r} (gas displacing water), θ_{go}^{a} (oil displacing gas), θ_{go}^{r} (gas displacing oil).

There is an ambiguity in defining a third contact angle from Eq. (7) if advancing and receding values are different. For instance, imagine water is being injected into oil and gas where the appropriate gas-water and oil-water contact angles to be used are θ_{gw}^{a} and θ_{ow}^{a}, respectively. Now if one uses Eq. (7) to find the third contact angle θ_{go}, it is not clear that the calculated value is the advancing or receding gas-oil contact angle. This problem is also evident when one uses Eqs. (8) and (9), where it is not known, for example, which oil-water contact angle, i.e., advancing or receding, should be used to calculate receding gas-oil contact angle needed, for example, in gas injection into oil and water.

In this paper we first decide on the values of two of the contact angles and then calculate the third one using Eq. (7). We use θ_{ow}^{r} and θ_{go}^{r} to calculate a θ_{gw}. We also use θ_{ow}^{a} and θ_{go}^{a} to find another value of θ_{gw}. The smaller of two values of θ_{gw} is considered as receding and the larger one as the advancing value. We always make sure in every single pore and throat, the receding contact angle for each phase is less than or equal to the advancing value, i.e., $\theta_{ij}^{r} \leqslant \theta_{ij}^{a}$.

D. Spreading and wetting layers

The representation of the cross section of a pore or throat a square or triangle clearly is not an accurate description of the highly irregular structure of real porous media. However, this description does allow phases to be present in layers occupying the corners when a non wetting phase fills the center of the element.

During primary drainage oil can occupy centers of the pore space, leaving water as a wetting layer in the corners. During subsequent cycles of water and/or gas injection these water layers are still present and maintain continuity of water.

After gas injection into an element containing oil in the center and water in wetting layers, gas will occupy the center and it is possible that oil will remain in a layer sandwiched between the gas and water. These are called *spreading* layers; as we discuss later their stability is related to the spreading coefficient, contact angles, corner angles, and capillary pressures, and are likely to be present in spreading systems.

A spreading system has $C_s=0$ and oil spontaneously forms layers between water and gas in the pore space. A nonspreading system has $C_s<0$ and while oil layers can also be present [43,105,106] they tend to be stable for more restricted range of capillary pressures. Also, we refer to wetting and spreading *layers*—these layers are typically a few microns in thickness and have a *non-negligible* hydraulic conductivity and maintain phase continuity. In contrast *films* are of molecular thickness (of order a nanometer) and have *negligible* conductivity and do *not* contribute to phase continuity—where present films simply modify the apparent, or equilibrium, interfacial tensions, as discussed above.

IV. PREVIOUSLY DEVELOPED THREE-PHASE NETWORK MODELS

Heiba *et al.* [107] extended statistical network modeling previously used for two-phase systems [108,109] to three-phase flow. A Bethe lattice, or Cayley network was used to represent the porous medium. Relative permeabilities were calculated using Stinchcombe's formula [110] using series approximations from percolation theory. Only a single phase could occupy a throat. A given fluid was considered to be able to flow only when the site that it occupied was a member of a continuous flow path from inlet to the outlet. The displacement of one phase by another was controlled by accessibility and local entry capillary pressure. Six groups of displacement were considered: gas into oil, oil into gas, gas into water, water into gas, water into oil, and oil into water. Two spreading systems were investigated where in the first one gas and water were displacing oil while in the second case water and oil were displacing oil and gas. The results showed that the gas and water relative permeabilities were functions of only their own saturations. Oil layers prevented the direct contact of gas and water. Oil isoperms were found to be strongly curved, meaning that the oil relative permeability was not only a function of its own saturation. Extensions of the theory to handle the complications involved by the effects of wettability and phase swelling due to mass transfer were also discussed. It was concluded that three-phase relative permeabilities are generally path functions rather than state functions (function of saturation only) except in particular situations such as when two phases are separated by the third. This model used rather simple networks and displacement rules.

Soll and Celia [111] developed a computational model of capillary-dominated two- and three-phase movement at the pore level to simulate capillary pressure-saturation relationships in a water-wet system. Regular two- or three-dimensional networks of pores, connected to each other by throats, were used to represent the porous medium. Hysteresis was modeled by using advancing and receding values

for the contact angles for each pair of fluids. Every pore was able to accommodate one fluid at a time as well as wetting layers. Viscous forces were considered to be negligible but the effects of gravity were included to modify the local capillary pressures. In order to reproduce their micromodel experiments [37], oil as a spreading phase was allowed to advance ahead of a continuous invasion front. Several pores could be filled simultaneously. This model was the first to incorporate layer flow in three-phase network modeling albeit in a rather *ad hoc* fashion. The results were compared with capillary pressure-saturation results and fluid distributions from the two- and three-fluid micromodel experiments. The amount of oil layer flow was used as a fitting parameter. Predicted two-phase air-water and oil-water capillary pressures were in good agreement with measured values [37] although the model did not so successfully match three-phase data. The model was not used to calculate relative permeabilities.

Øren *et al.* [112] described details of the pore level displacement mechanisms taking place during immiscible gas injection into waterflood residual oil (tertiary gas injection) which then were incorporated into a two-dimensional strongly water-wet square network model with rectangular links and spherical pores in order to compute oil recovery in spreading and nonspreading systems. Simulated recoveries compared very well with the measured values from micromodel experiments [35,113]. The authors described a double drainage mechanism where gas displaces trapped oil that displaces water allowing immobile oil to become connected boosting oil recovery. Oil recovery decreased with decreasing spreading coefficient. In nonspreading systems, the probability of direct gas-water displacement was high and capillary fingering of gas resulted in early gas breakthrough and low oil recovery. In spreading systems oil reconnection was more effective and direct gas/oil displacement was preferred. It was concluded that a simple invasion percolation algorithm [114,115] including the spreading layers works well in mimicking the complex three-phase behavior seen in micromodels. In this work relative permeabilities were not calculated.

Pereira *et al.* [28] developed a dynamic two-dimensional network model for drainage-dominated three-phase flow in strongly water- and oil-wet systems when both capillary and viscous forces were important. The displacement mechanisms in spreading and nonspreading systems were described by generalization of two-phase displacement mechanisms. Both pores and throats were assumed to be lenticular in cross section allowing wetting and spreading layers to be present. The simulated recoveries at gas breakthrough were compared against measured values in micromodels [35]. As in Øren *et al.* [112], a large difference between the recoveries in spreading and nonspreading systems was reported for water-wet cases due to existence of oil layers in the spreading systems. The highest recovery, 85%, was found for the oil-wet case. This was because continuous wetting layers prevented trapping of oil. The oil recovery was much lower, 14%, for the water-wet case in a nonspreading system. This was because there were no spreading layers of oil. Even when layers were present for the spreading system, the oil recovery was much lower, 40%, in a water-wet medium than for the oil-wet case. Water in water-wet systems played the same role as oil in oil-wet systems—water recoveries in water-wet spreading and nonspreading systems were high. An order of magnitude reduction in the simulated conductivity of the oil layers decreased oil recovery and made the behavior of the spreading system similar to that of a nonspreading system. Also a reduction in initial oil saturation for tertiary gas injection decreased the oil recovery. This was true for both spreading and nonspreading systems indicating that the recovery of the intermediate wetting phase is strong function of saturation history. This was reported to be consistent with experiments by Dria *et al.* [3] and Oak [116,117]. It was also concluded that the recovery of the wetting fluid is independent of the saturation history. Relative permeabilities were not calculated in this work.

Paterson *et al.* [118] developed a water-wet percolation model to study the effects of spatial correlations in the pore size distributions on three-phase relative permeabilities and residual saturations. This was an extension of their previous work on two-phase systems [119]. Fractal maps derived from fractional Brownian and Levy motion (fBm and fLm) were used to assign pore size. A simple site percolation model with trapping was used. Trapping was incorporated based on Hoshen-Kopelman algorithm [120]. In three-phase simulations direct displacement of oil and water by gas and also double drainage were implemented. The model assigned the same volume to all pores and so the fraction of sites occupied by a phase gave its saturation. All the sites were assumed to have the same conductivity regardless of their radii. The simulation results for correlated properties showed lower residual saturations in comparison to uncorrelated ones. Incorporating a bedding orientation to the spatial correlations had a major impact on relative permeability. When the bedding was parallel to the flow direction, the relative permeabilities were greater and residual saturations lower than those when bedding was perpendicular to the flow. This was also the case for two-phase relative permeabilities [119]. The effects of spreading coefficient were also studied. Similar to previous authors [28,112] it was shown that the less negative the spreading coefficient, the lower the final residual oil saturation. For more negative spreading coefficients direct gas to oil and gas to water displacements are preferred over double drainage. This effect was more significant for correlated systems.

Fenwick and Blunt [88,89] developed a three-phase network model for strongly water-wet systems. A regular cubic network composed of pores and throats with equilateral triangular or square cross sections was used. Oil-water and gas-water contact angles were considered to be zero. Two- and three-phase displacement mechanisms including oil layer flow observed in micromodel experiments were incorporated in the model. Double drainage was generalized to allow any of six types of double displacement where one phase displaces a second that displaces a third as observed by Keller *et al.* [43]. The model was able to simulate any sequence of oil, water, and gas injection. Using a geometrical analysis, a criterion for stability of oil layers was derived which was dependent on oil-water and gas-oil capillary pressures, contact angles, equilibrium interfacial tensions, and the corner half angle. It was argued that oil layers could be

present even for negative spreading coefficient systems. Using a simple calculation [94] it was shown that the layers are of order a micron across or thicker in the corners, roughness, and grooves of the pore space. The work estimated conductance of an oil layer which then was used to compute oil relative permeability. It was shown that at low oil saturation the oil relative permeability should vary quadratically with saturation, as observed experimentally [121–124]. An iterative methodology which coupled a physically based network model with a one-dimensional (1D) three-phase Buckley-Leverett simulator was developed in order to find the correct saturation path for a given process with known initial condition and injection fluid [88]. This enabled the network model to compute the properties for the right displacement sequence. Relative permeabilities for secondary and tertiary gas injection into different initial oil saturations were presented. The resultant saturation paths compared well qualitatively with experimental data by Grader and O'Meara [121]. The paths in the oil-water vs gas-oil capillary pressure space were all located in the region where oil layers were stable meaning that oil did not get trapped. Oil relative permeabilities for different initial conditions were different from each other, consistent with several experimental studies [2,14,117,125,126].

Mani and Mohanty [127,128] also used a regular cubic network of pores and throats to simulate three-phase flow in water-wet systems. Pores and throats were considered to be spherical and cylindrical, respectively. The oil-water capillary pressure was fixed at its original value during the gas invasion processes. The parameters of the network were tuned to match two-phase mercury-air experimental capillary pressures for Berea sandstone [129].

Both dynamic and quasistatic simulations were carried out. The work had two important features: (i) dynamic simulation of capillary-controlled gas invasion, where it was assumed each phase pressure was not constant across the network; (ii) re-injection of the produced fluids at the outlet of the medium into the inlet in order to simulate larger systems. This was used to see whether trapped oil ganglia become reconnected by double drainage to form spanning clusters. The two-phase processes were simulated at low capillary number using traditional quasistatic assumptions. Pressure drops across pores were ignored. The model included fluid flow through wetting and spreading layers. A fixed conductance was assigned to oil layers. For the capillary pressure histories used, no stable oil layers were observed in both spreading and nonspreading systems. Gas invasion was modeled by three displacement mechanisms: direct gas-water, direct gas-oil, and double drainage. For each displacement a potential was considered which was the difference between the pressures of two involved fluids minus the threshold capillary pressure of the displacement. The displacement with the largest potential was carried out first. Re-injection of fluids was simulated by replacing the fluid distribution in the inlet zone by the fluids in the outlet zone. The process was terminated after steady state was reached at the imposed pressure conditions, i.e., when no further gas invasion was possible at the imposed capillary pressure. The final oil saturation in spreading systems was zero. The capillary pressure curves obtained from dynamic and quasistatic simulations were virtually identical. For nonspreading systems with a low oil-water capillary pressure, drainage of water and oil occurred with similar probability. The effect of spreading coefficient and saturation history on three-phase relative permeability was consistent with other network modeling studies [28,88,89,112] and experimental measurements [2,14,117,125,126].

Laroche *et al.* [130,131] developed a pore network model to predict the effects of wettability heterogeneities with different patterns and spatial distributions on displacement mechanisms, sweep efficiency, and fluid distribution in gas injection into oil and water. A dalmatian type of wettability heterogeneity was used with continuous water-wet surfaces enclosing discontinuous regions of oil-wet surfaces or vice versa. A series of three-phase glass micromodel experiments with different wettabilities were also carried out. Measured oil-water contact angles for the water-wet and oil-wet surfaces were 0° and 105°, respectively. *n*-dodecane, water, and nitrogen were the three fluids used in the experiments. All the two-phase interfacial tensions, densities, and viscosities were measured. The initial spreading coefficient was 7.3 mN/m and hence the oil was assumed to be spreading. The capillary number throughout the experiments was approximately 10^{-5} indicating capillary controlled displacement. A 2D regular pore and throat network was used to simulate the experiments. All the throats had triangular cross sections while the pores were circular cylinders. The pore and throat size distributions were similar to those of Berea sandstone. Saturations, conductances, and relative permeabilities were calculated using similar techniques to Fenwick and Blunt [89]. The fluid distributions at the end of two- and three-phase simulations were in good qualitative agreement with those found experimentally.

Hui and Blunt [132] developed a mixed-wet model of three-phase flow for a bundle of capillary tubes. The tubes had different sizes and were equilateral triangle in cross section. Wettability alteration was modeled by changing the wettability of surfaces that came into contact with oil after primary drainage. The model simulated three-phase flow with any combination of oil-water, gas-water, and gas-oil contact angles. In all some ten fluid configuration were considered. Primary drainage, water flooding, and tertiary gas injection were simulated. The effects of wettability, spreading coefficient, and initial oil saturation on relative permeabilities were investigated. Possible configuration changes during each process along with the threshold capillary pressure of each change were presented. The stability of layers in different configurations and capillary pressures at which they collapse was discussed. We will extend this approach to study 30 different possible fluid configurations in three-phase flow and will incorporate them in a three-dimensional random network model.

Lerdahl *et al.* [133] used the technique developed by Bakke *et al.* [47] to reconstruct a three-dimensional void space, Fig. 1, and then convert it to a pore and throat network, Fig. 2, for use in a water-wet network model to study drainage-dominated three-phase flow. Simulated results were compared successfully against the experimental data by Oak [117]. We will use a similar network in our studies and also compare our predictions against Oak's experiments [117]. In

our study we will compare results on a point-by-point basis using our saturation tracking algorithm and extend the model to mixed-wet systems following the approach of Hui and Blunt [132].

Larsen *et al.* [90] used a water-wet three-dimensional cubic pore network model based on the work of Fenwick and Blunt [88,89] to simulate a series of micromodel experiments of WAG (water alternate gas) injection processes. All the pores and throats were assumed to have square cross sections. The network model was used in an iterative procedure similar to the one used by Fenwick and Blunt [88] to find self-consistent saturation paths. Three WAG injections with different gas-water injection ratios were carried out.

Van Dijke *et al.* [97,134,135] presented a process-based mixed-wet model of three-phase flow using a bundle of capillary tubes with circular cross sections to study the saturation dependencies of capillary pressures and relative permeabilities for spreading and nonspreading systems. Larger pores were considered to be oil-wet and the smaller ones water-wet. It was shown that based on interfacial tensions and contact angles the three-phase saturation space could be divided up to three different regions with a different intermediate-wet phase. The relative permeability of this phase was a function of two saturations. Also the capillary pressure between the most wetting and nonwetting phases is dependent on two saturations. The relative permeabilities of the other two phases were a function of only their own saturation in this region.

Van Dijke *et al.* [86,87] developed a regular three-dimensional three-phase network model for systems with different wettability expanding on their previous studies on bundles of capillary tubes. Every element was allowed to have a different oil-water contact angle and Eqs. (8) and (9) were used to determine the gas-oil and gas-water contact angles [97]. While layers were not incorporated explicitly in saturation or conductance computations they were allowed to establish continuity of different phases. The model was a cubic array of only throats with a circular cross section. The coordination number could be changed by removing throats from the network. An extensive series of simulations of three-phase flow was performed. For networks with a high coordination number, the saturation dependencies were qualitatively similar to those predicted for capillary bundles. As the coordination number was reduced, connectivity was impaired and trapping became significant. They compared their network simulations with micromodel experiments of WAG [136,137] where there were repeated cycles of water and gas flooding. To reproduce the results they incorporated multiple displacements where a train trapped clusters may displace each other until there is invasion into a connected phase. They suggested that such multiple displacements were significant in WAG flooding. While certainly such displacements were observed in the micromodel experiments, we suggest that in three-dimensional displacements the phases are likely to be better connected and so the movement of trapped ganglia is less significant. We will only consider double displacements in this paper.

While many three-phase pore-scale displacement mechanisms are well understood, and the generic functionality of relative permeability has been discussed, three-phase network models to date have not addressed the full range of possible configurations in mixed-wet systems and their predictive powers are limited. The network model described here combines three essential components: (i) a description of the pore space and its connectivity that mimics *real* systems; (ii) a physically-based model of *wettability alteration*; and (iii) *a full description of fluid configurations* for two- and three-phase flow. This will enable us to predict three-phase three-phase relative permeabilities for media of arbitrary wettability using geologically realistic networks.

V. MODEL ASSUMPTIONS

In this work, it is assumed that the fluids are Newtonian, incompressible, and immiscible. It is also assumed that the capillary number

$$N^{cap} = \frac{\mu \nu}{\sigma}, \tag{10}$$

where μ is the viscosity and ν is the fluid velocity, to be low enough, i.e., $10^{-6}-10^{-7}$ and smaller, such that the system is in capillary equilibrium and fluid flow is capillary controlled at the pore scale. This is a reasonable assumption for most reservoir displacements away from the well bore [89,133].

The Bond number is a ratio of gravity to capillary forces:

$$B = \frac{(\rho_i - \rho_j) g L^2}{\sigma_{ij}} (ij = ow, gw, go), \tag{11}$$

where ρ is the density, L is a typical pore length, and g is the acceleration due to gravity. We can neglect gravity if the Bond number is less than 10^{-4}, which again is satisfied for most pore-scale displacements [4].

We further assume there is no momentum transfer across the fluid-fluid interfaces. As in Zhou *et al.* [138], in our computations of phase conductance we consider free boundaries for gas-oil and gas-water interfaces and no-flow for water-oil interfaces. When there is continuity of velocity across the interfaces, the pressure gradient in one phase may affect the flow and consequently the relative permeability of the other phases. This phenomenon for two-phase flow has been investigated by Goode and Ramakrishnan and Kalaydjian [91,139]. We will ignore this complication in this work.

To find the pressure difference across an interface we use the Young-Laplace equation:

$$P_i - P_j = \sigma_{ij} \left(\frac{1}{r_1} + \frac{1}{r_2} \right), \tag{12}$$

where r_1 and r_2 are the principal radii of curvature, and P_i and P_j are pressures of the phases on either sides of the interface.

There are two types of interface: (i) *Main terminal meniscus (MTM)* [85], which is the invading meniscus at the pore-throat junction separating wetting and nonwetting fluids. The shape of such a meniscus is assumed to be spherical meaning that the two radii of curvature are the same ($r_1 = r_2 = r$). The pressure difference across an MTM is then given by

$$P_i - P_j = \frac{2\sigma_{ij}}{r}. \tag{13}$$

(ii) *Arc meniscus (AM)*, which is the interface at a corner of a noncircular element. It is assumed that the curvature of the interface is negligible parallel to a pore or throat meaning that the principal radii of curvature would be $r_1 = r$ and $r_2 = \infty$ [85,93]. The pressure difference across such an interface is given by

$$P_i - P_j = \frac{\sigma_{ij}}{r}. \tag{14}$$

As Lerdahl *et al.* [133], the clay volume associated with each pore and throat in the network is considered to be full of water and immobile. It is also assumed that fluids have been long enough in contact to keep the level of solubility of one fluid in the other constant throughout all the processes. Temperature is also fixed to prevent changes in solubility of fluids in each other. These two assumptions ensure that interfacial tensions stay the same during different processes.

For each displacement event we also assume that every interface is comprised of only two phases [37,111]. Only the saturation of the invading phase whose pressure increases is allowed to increase while the two other saturations are either constant or decrease [111].

VI. PORE-SCALE NETWORK MODELING

The model assumes quasistatic displacement controlled, at the pore scale, entirely by capillary forces. The simulation proceeds as a series of displacements. A displacement is the change of the configuration group(s) in one pore or throat (see details later). This can represent the replacement of one phase by another in the center of the pore, or the collapse or formation of a layer in a single corner. There is a capillary pressure associated with the transition from one configuration to another. We define pressures of water, oil, and gas in the network. As displacement proceeds, these pressures will increase.

A. Primary drainage and wettability alteration

The network is initially fully saturated with water and strongly water-wet, with the oil-water contact angle $\theta_{ow}^{PD} = 0$ and all phase pressures are set to zero. Oil then enters the network and it invades the pore or throat with the lowest capillary entry pressure and changes the configuration groups in an invasion percolation process [114,115]. Drainage is complete when a target capillary pressure or saturation has been reached, or when all pores and throats have been invaded by oil.

At the end of primary drainage, regions of the pore space in direct contact with oil may change their wettability. We assign an advancing oil/water contact angle θ_{ow}^{a} to each oil-filled pore and throat after primary drainage. Different pores and throats may have different contact angles. Contact angles are assigned at random to oil-filled pores and throats, according to some specified distribution. In this paper, the contact angles will have a uniform distribution between some specified maximum and minimum values.

After primary drainage, the model simulates any sequence of water, gas and/or oil invasion.

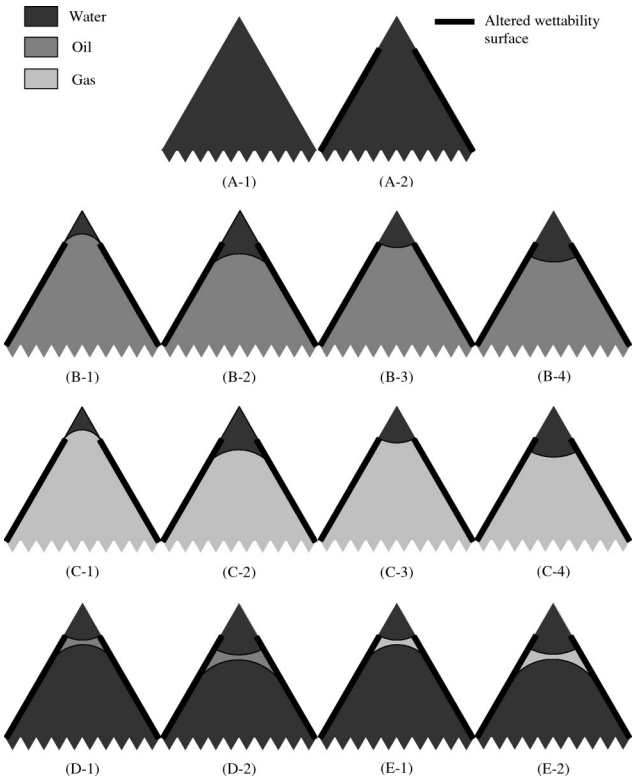

FIG. 6. One and two phase configurations for a single corner. The bold solid line indicates regions of the surface with altered wettability. All the multiphase contact points may be pinned which means that as the capillary pressure changes, the curvature of the interface changes but that the location of the interface-solid contact is fixed. A phase may be present in the center of the pore space or as a spreading or wetting layer, sandwiched between other phases. Water is always present in the corner. The network model simulates a sequence of displacement events that represent the change from one configuration to another. Tables VIII-XIV in Appendix C list the capillary pressures for each displacement.

B. Two- and three-phase fluid generic configurations

Different oil-water, gas-water, and gas-oil contact angles and interfacial tensions make it theoretically possible to accommodate fluids in the corners of the pore space with different configurations. Figures 6 and 7 illustrate possible generic configurations of one, two, or three fluids in a single corner of an angular pore or throat with any values of two- and three-phase contact angles—the whole pore or throat is composed of no (circle), three (triangular), or four (square) corners. The configurations are equally applicable for any other angular pore or throat with any number of corners. Altered wettability surfaces are shown by thicker lines. Fluid located in the corner, layer, or center of a configuration is called a *phase location*. For example, configuration group *F* has three phase locations, water in a corner, an oil layer, and gas in the center. For single phase configurations—group A—only one phase location, i.e., water in the center, is considered. Every phase location has a flag associated with it indicating whether the fluid that it accommodates is *continuous* or *trapped*. A cluster of phase locations is trapped when it does not connect to the inlet and outlet; if it does then it is

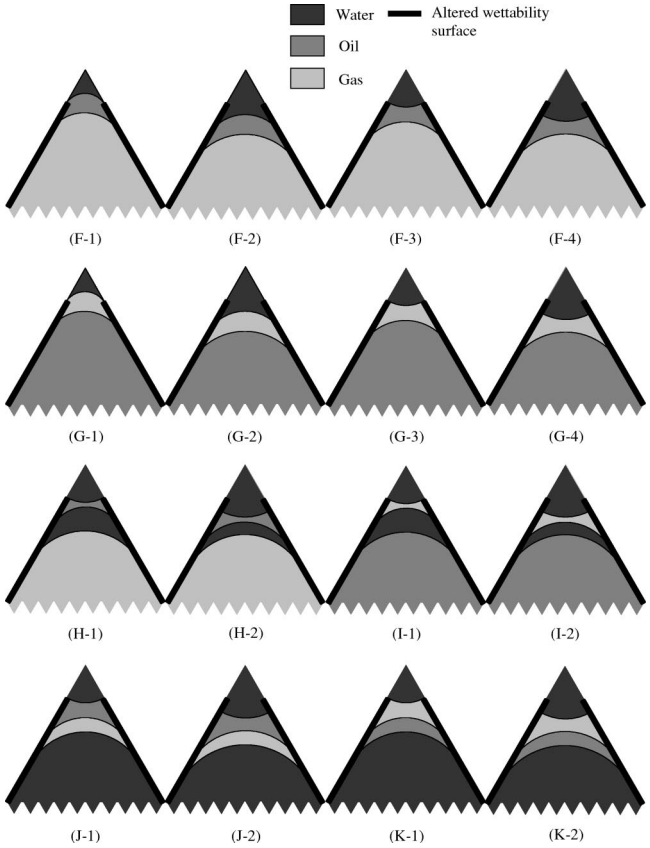

FIG. 7. Three phase configurations for a single corner, continued from Fig. 6.

considered continuous. We shall discuss the details of how the phase locations are assigned to the clusters and how their continuity is determined later in this paper.

For elements with a circular cross section, only one phase may occupy the pore or throat. For square and triangular cross sections, the phase in the middle of the element must be the same for each corner, but different corners may have different configurations, depending on the corner angle. However, in a single pore or throat, the contact angles in each corner are the same. Table III lists the range of contact angles for which each configuration in Figs. 6 and 7 may exist. A capillary pressure between any two phases, i.e., P_{cij}, is defined as $P_i - P_j$. The radius of curvature r of the interface between two phases i and j in Figs. 6 and 7 is related to the capillary pressure by Eq. (14).

One should note that when Eq. (14) is applied to calculate radius of curvature for an interface, P_i and P_j may be different from the inlet or outlet pressures, i.e., the *global* absolute pressures of the two phases, if that phase is trapped. In such cases the absolute pressures of the trapped clusters are used.

Capillary pressure is used in this paper in two senses. The first is a threshold or entry capillary pressure at which a displacement in an element occurs. This has a precise definition dependent on the contact angles and pore geometry. The second is when there is some imposed pressure differences between phases in an element that is used to determine the radius of curvature of interfaces. This pressure difference always corresponds to a threshold capillary pressure for a recent displacement.

TABLE III. The range of contact angles for which each configuration in Figs. 6 and 7 can exist.

Configuration	θ_{ow}	θ_{gw}	θ_{go}
A-1, A-2			
B-1, B-2	$< \pi/2 - \alpha$[a]		
B-3, B-4	$\geqslant \pi/2 - \alpha$		
C-1, C-2		$< \pi/2 - \alpha$	
C-3, C-4		$\geqslant \pi/2 - \alpha$	
D-1, D-2	$\geqslant \pi/2 + \alpha$		
E-1, E-2		$\geqslant \pi/2 + \alpha$	
F-1, F-2	$< \pi/2 - \alpha$		$< \pi/2 - \alpha$
F-3, F-4	$\geqslant \pi/2 - \alpha$		$< \pi/2 - \alpha$
G-1, G-2		$< \pi/2 - \alpha$	$\geqslant \pi/2 + \alpha$
G-3, G-4		$\geqslant \pi/2 - \alpha$	$\geqslant \pi/2 + \alpha$
H-1, H-2	$\geqslant \pi/2 + \alpha$	$< \pi/2 - \alpha$	
I-1, I-2	$< \pi/2 - \alpha$	$\geqslant \pi/2 + \alpha$	
J-1, J-2	$\geqslant \pi/2 - \alpha$	$\geqslant \pi/2 + \alpha$	$< \pi/2 - \alpha$
K-1, K-2	$\geqslant \pi/2 + \alpha$	$\geqslant \pi/2 - \alpha$	$\geqslant \pi/2 + \alpha$

[a]Corner half angle.

C. Definitions

A *displacement* is defined as a change in generic configuration groups (indicated by letters in Figs. 6 and 7) in an element by an *eligible* displacing phase which is the phase residing in a phase location that is topologically capable of doing the change(s). Based on the type of displacement this can be a configuration change in one or all corners of the element. For every configuration change, there might be *different* ways to carry out the displacement. In such a case each one is treated as a *separate* displacement. For instance, imagine configuration group change *F* to *C* due to oil layer collapse. The change could be carried out either by invasion of water in the corner or gas in the center which corresponds to a decrease in P_{cow} or an increase in P_{cgo}, respectively. These two ways are treated as two separate displacements. The network model simulates a sequence of displacements induced by imposed changes in phase pressures.

For every displacement, there are two phase locations associated with it. One accommodates the displacing fluid of the displacement, the *displacing phase location*, and the other one accommodates the displaced fluid, the *displaced phase location*. For example, consider configuration group change B to C by an invasion of gas residing in the center of a neighboring pore into oil in the center of a throat. The displacing and displaced phase locations for this displacement are the gas center in the pore and the oil center in the throat, respectively.

A *process* is defined as a consecutive sequence of displacements that involve a change in the same capillary pressure in the same direction. The change in capillary pressure, P_{cij}, is due to injection of either phase i or j. For instance, primary drainage is a process involving an increase in oil-water capillary pressure. Water flooding is a different process involving a decrease in oil-water capillary pressure.

Drainage in a capillary element is referred to an event

where a *wetting* phase is displaced by a *nonwetting* phase. An event in which a *nonwetting* phase is displaced by a *wetting* phase is called *imbibition*.

Because of contact angle hysteresis, the contact angle can hinge between its receding and advancing values without the contact line moving and is called the *hinging* contact angle. Every interface has two contact angles associated with it: (i) a *target* contact angle, which is the contact angle that the *new* AM's will have just after a displacement in that element. The *existing* (old) AM's *might* reach this value just before displacement. This contact angle may be different from one process to another. For example, imagine a configuration group change A to B by oil primary drainage. The new AM's in configuration group B will have the target contact angle of θ_{ow}^{PD}. The target contact angle during water flooding for an existing oil-water interface in configuration group B is θ_{ow}^{a}. (ii) the *furthest* contact angle, which is the maximum, or minimum, hinging contact angle that an interface reached during the last process when the pertinent capillary pressure was changing. This may not necessarily be the same as the target contact angle. For instance, imagine water flooding is being carried out after primary drainage in a strongly oil-wet system with $\theta_{ow}^{a}=\pi$. When the oil-water capillary pressure decreases the oil-water AM's start hinging from θ_{ow}^{PD} towards the target contact angle θ_{ow}^{a}. If water flooding is stopped at some stage then there might be AM's, particularly in wide corners, that have not reached the advancing value yet. For such AM's the last hinging contact angles are considered as their furthest contact angles. For the AM's that reached the target contact angle, the furthest contact angle will be the same as the target contact angle. For the next process, for instance gas injection, the interface may start hinging from this furthest value towards the new target contact angle.

Every AM has a meniscus-apex distance b associated with it (see Fig. 14 in Appendix A), and is calculated using Eqs. (C5) and (C6) with θ_1 being the angle that the AM makes with the surface towards the apex, α the corner half angle, σ the interfacial tension, and $P_{c,extreme}$ the capillary pressure of the last move of the AM. b changes whenever the AM moves.

D. Basic displacements

Displacements may be categorized into four groups:

(i) *Pistonlike*, which refers to the displacement of one phase by another in the center of a throat by a fluid residing in the center of a neighboring pore. The prevailing contact angles during drainage and imbibition events are receding and advancing values, respectively. If there is no contact angle hysteresis then the threshold capillary pressure of pistonlike imbibition is the same as that of drainage, otherwise during imbibition the relevant capillary pressure is reduced and each interface starts hinging from its furthest value towards the advancing contact angle. It stays pinned as long as the hinging value is smaller than the advancing contact angle. The wetting phase will enter the element when the advancing contact angle is reached. The threshold capillary pressures are found using the Mayer-Stowe-Princen (MSP) theory [48,140–143].

(ii) *Pore-body filling* refers to the displacement of one phase in the center of a pore by movement from the center of the adjoining throat(s). For drainage the threshold capillary pressure is given by similar expressions for pistonlike advance. For imbibition threshold capillary pressure depends on inscribed radius of the porebody and the number of neighboring throats that either do *not* hold the invading phase in the center or cannot *contribute* to the displacement because they are trapped. For a pore with coordination number m, $m-1$ pore-body filling events are possible, called I_n, where n is the number of neighboring throats that are not involved in the displacement $1 \leqslant n \leqslant m-1$ [29,30]. When $n=1$, the displacement is a pistonlike event with the corresponding threshold capillary pressures [29,48]. The equations to compute threshold capillary pressures for pistonlike and pore-body filling displacements are listed in Tables VIII–XI in Appendix C.

(iii) *Snapoff* corresponds to an event where the phase in the center of a pore or throat is displaced by a phase residing in corners or layers. When the relevant capillary pressure decreases the invading phase starts swelling and consequently contributing AM's—starting from the sharpest corner—may hinge and eventually move—when the hinging contact angle reaches the advancing value—towards the center to meet the other moving or pinned AM's. When AM's meet the center of the element is filled spontaneously by the displacing phase. Depending on the magnitude of the advancing contact angle snapoff can be spontaneous ($\theta^a \leqslant \pi/2-\alpha_1$) or forced ($\theta^a > \pi/2-\alpha_1$). Snapoff is not favored over a pistonlike or pore-body filling event when there is a neighboring element with the invading phase in the center that is able to carry out the displacement. The threshold capillary pressures are found using the equations tabulated in Tables XII and XIII in Appendix C.

(iv) *Layer collapse and formation*, pistonlike, and snapoff displacements—if the pertinent contact angles, capillary pressures, and corner half angles permit—allow the displaced phase to remain as layer(s) sandwiched between fluids in the corner(s) and center of the element. The formation of layers in an element is also possible by displacement from fluids residing in the *layers* or *center* of the neighboring elements. The layers may collapse by an increase in pressure of the fluids on either side of the layer. When a layer collapse event takes place, one of the two AM's bounding the layer will hinge and/or move towards the other one. However, sometimes both AM's contribute into the layer collapse event, e.g., oil layer collapse event by water in configuration group D. Expressions to compute threshold capillary pressures are listed in Table XIV in Appendix C.

E. Configuration changes

Configuration changes make it possible to simulate any sequence of fluid injection in two- and three-phase systems. All possible changes are displayed in Figs. 8–12.

Here we present points that one should consider to record configuration changes:

1. After every configuration group change, there will be some new displacements to be considered. These displace-

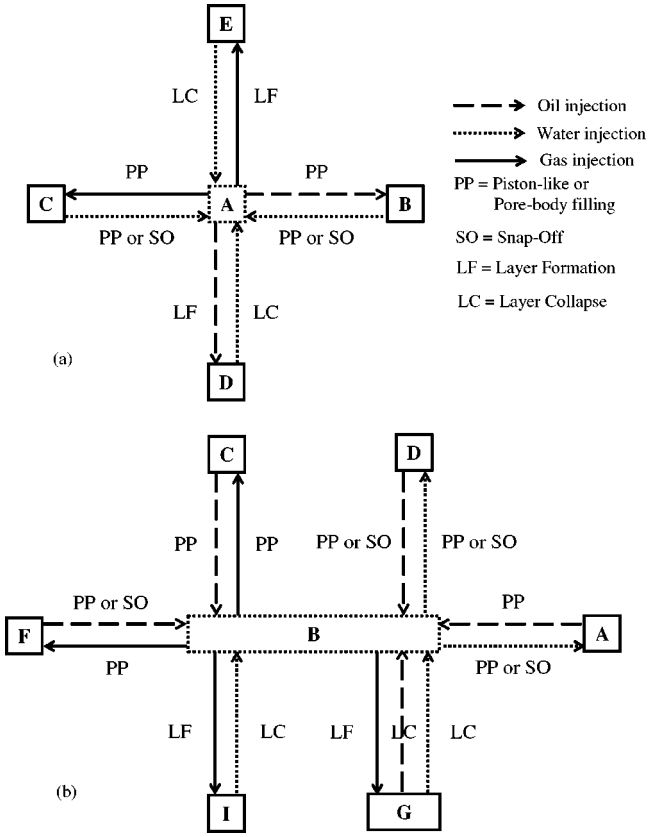

FIG. 8. Possible configuration changes to configurations (a) A and (b) B.

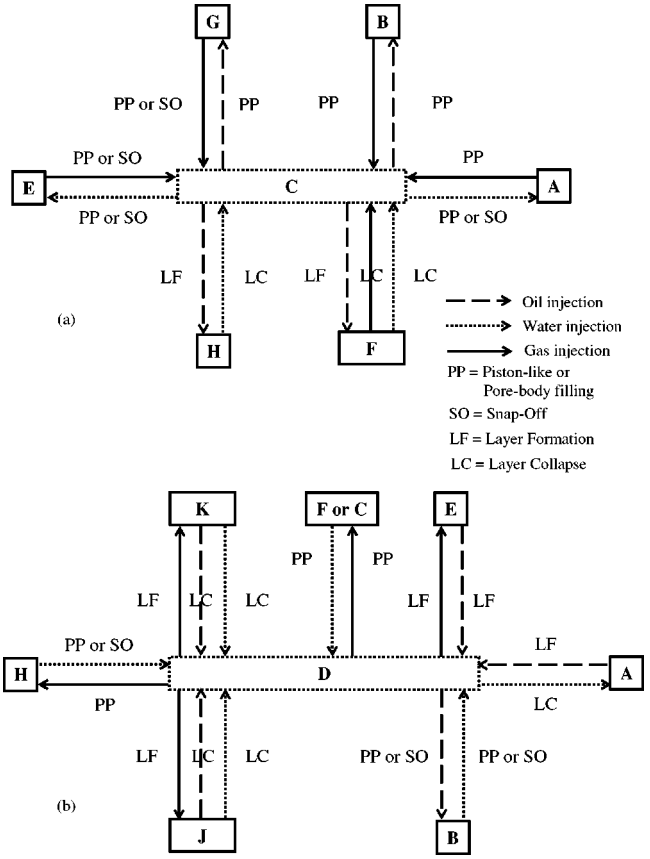

FIG. 9. Possible configuration changes to configurations (a) C and (b) D.

ments are added into the *appropriate* lists (see details later). For every new displacement, the appropriate list is determined knowing what phase is displacing and whether the phases occupying the displacing and displaced phase locations are continuous or trapped.

2. Once a configuration group is changed, the type and the number of AM's in the corner may also change. There are two possibilities: (i) the number of AM's is the same but the type has been changed—fluid on one side of the AM has been replaced by a new fluid. For example, consider configuration group change B to C. In this case the furthest contact angle of the AM before the configuration change is given to the AM after the configuration change and then the interface may hinge from its furthest value towards the target contact angle (due to changes in the pertinent capillary pressure) and ultimately move. This will prevent any volume error of the fluid residing on the other side of the AM—i.e., water in the corner in the example above. We call this case an *old* AM case. (ii) the number of AM's in the corner has either increased or decreased. If it has increased by pistonlike or snapoff displacement then the *new* AM will have the furthest contact angle the same as the target value and moves according to the changes in the relevant capillary pressure. For example, imagine configuration group change B to F by pistonlike invasion of gas. The furthest contact angle of the new gas-oil AM will be θ^r_{go}. If the number of AM's has increased by layer formation, see point 4. Finally if the number of AM's has decreased (by layer collapse) then it is treated as an old AM case. An example is the gas layer collapse event by water or oil in configuration group G to form an oil-water AM in configuration group B.

3. An AM moves once the hinging contact angle becomes as large as the advancing contact angle of the AM (when the related capillary pressure is decreasing) or as small as the receding contact angle of the AM (when the related capillary pressure is increasing). Once the AM moves, the new b is calculated. The value of b is updated as long as the AM keeps moving by changes in the pertinent capillary pressure in the same direction as when it started to move.

4. When a new layer formation event is considered, there are two displacements that may represent such an event and both must be added to the lists. Imagine an AM where a layer is going to be formed around it. The first displacement may displace some of the fluid above the AM to accommodate the layer while the other one displaces some of the fluid below the AM to make space for the layer. For example, consider gas layer formation resulting in configuration group change B to G. The two displacements may take place only if $\theta^r_{go} > \pi/2+\alpha$. By the first one, gas may displace some of the water in the corner to open enough space for the layer while forming a new gas-water interface for which the meniscus-apex distance b is calculated. Both target and furthest contact angles of the gas-water interface will be θ^r_{gw}. One should note that the gas-oil interface, in the new configuration, is treated as an old AM. π minus the furthest contact angle of the oil-water interface before the configuration group change

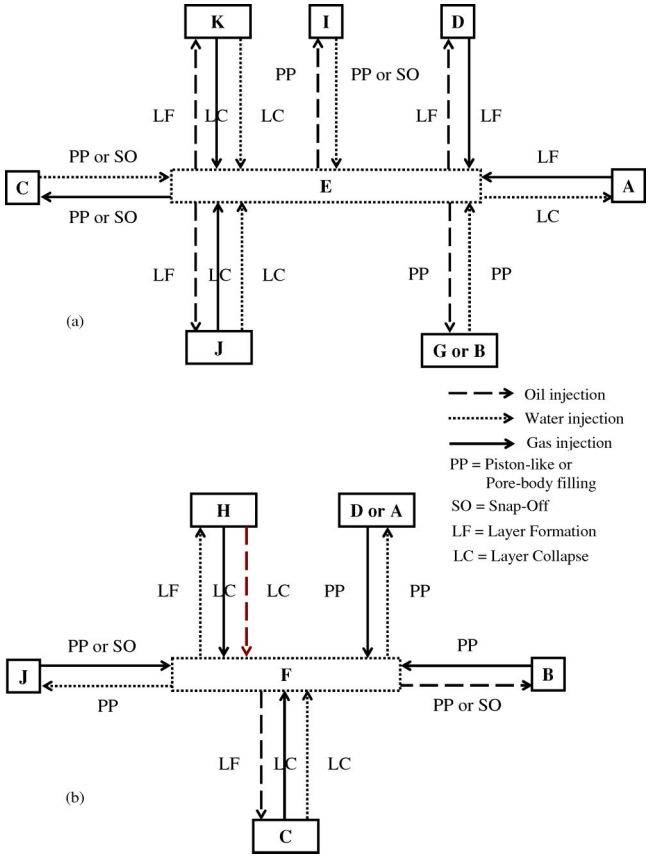

FIG. 10. Possible configuration changes to configurations (a) E and (b) F.

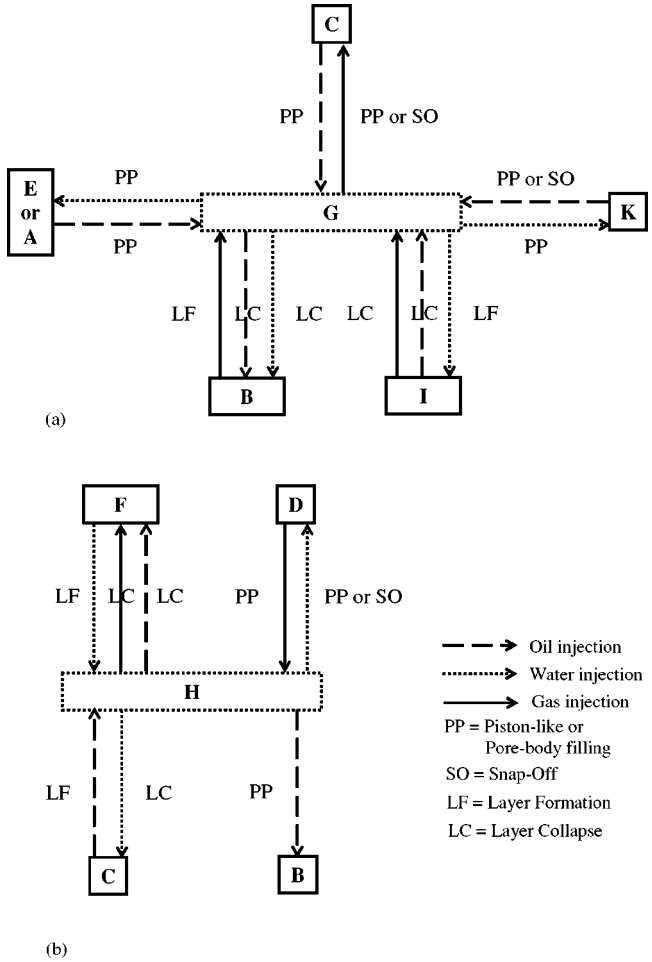

FIG. 11. Possible configuration changes to configurations (a) G and (b) H.

is given as the furthest contact angle of the gas-oil interface. Then the gas-oil interface may start hinging from its furthest value towards θ^r_{go} if the gas-oil capillary pressure is increased during the process. Also the meniscus-apex distance b of the oil-water interface is given to the gas-oil interface. The threshold capillary pressure of the layer formation is calculated using θ^r_{gw} and the furthest value of the gas-oil interface. But in the second displacement, gas may displace some of the oil in the center to accommodate itself as a layer. A new gas-oil interface is created and so its meniscus-apex distance b is calculated. Both target and furthest contact angles of the gas-oil interface will be θ^r_{go}. The gas-water interface is considered as an old AM and the furthest contact angle of the oil-water interface before the configuration change is used as the furthest contact angle of the gas-water interface. Then the gas-water interface may hinge from its furthest value towards θ^r_{gw} if the gas-water capillary pressure is increased during the process. Also the meniscus-apex distance b of the oil-water interface is given to the gas-water interface. The threshold capillary pressure of the layer formation is calculated using θ^r_{go} and the furthest contact angle of the gas-water interface.

5. Once a displacement changes a configuration group, there might be other displacements that had been considered for the same configuration group change but through other routes. These displacements are not valid anymore and are omitted from the lists.

6. New pistonlike displacements are considered only if the configuration group change has replaced the fluid at the center of the element and there is at least one different phase residing in the center of the neighboring elements.

7. New layer formation displacements are added to the lists only when the phase that is expected to form the layer is located in neighboring element(s) in the center or layer.

8. New snapoff displacements are added to the list as soon as a new AM is formed or the type of an old AM has changed. This is considered only if the fluid in the center of the element is residing on one side of the AM. A new layer collapse event is considered only if a new layer forms.

9. Once a new configuration group is formed, it might allow new displacements in the *neighboring* elements. For instance, imagine a pistonlike displacement by gas changes configuration group B to C in an element. Formation of a gas layer in the corners, as well as displacement of oil and water in the center, of the neighboring elements are considered if topological and contact angle circumstances permit.

10. There are some configurations (see Figs. 6 and 7) that have more than one AM. The AM's and also layers are numbered from the apex inwards.

F. Continuity and clustering

An algorithm to determine cluster distributions, critical percolation concentration, and percolation probabilities in

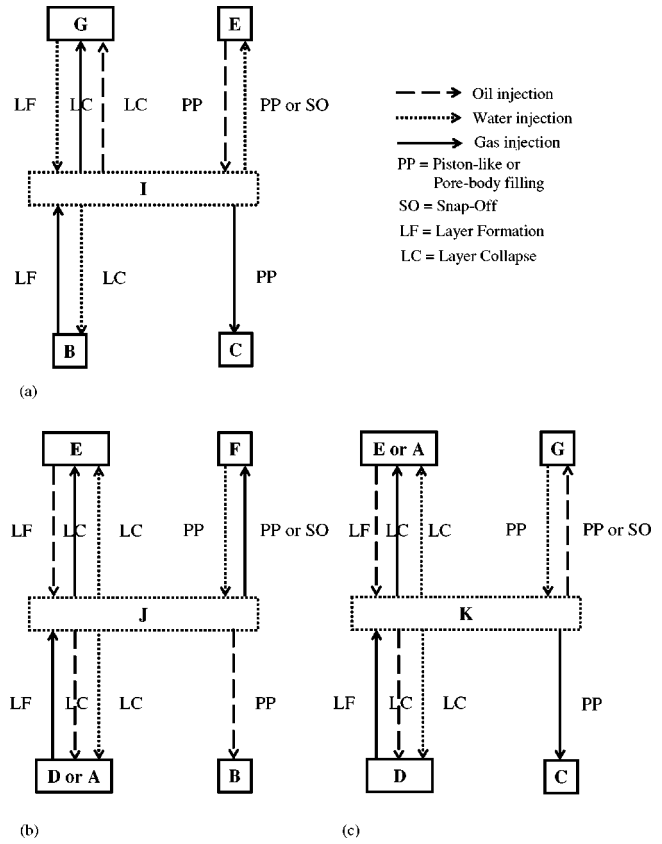

FIG. 12. Possible configuration changes to configurations (a) I, (b) J, and (c) K.

network modeling has been developed by Hoshen and Kopelman [120] which was later extended to irregular networks by Al-Futaisi and Patzek [144].

We use a different displacement-based algorithm to determine cluster distributions. It is applicable to any two- or three-dimensional regular and random network with any number of phases, i.e., phase locations, residing in a pore or throat. In contrast, the original Hoshen-Kopelman algorithm [120] assumed that only a single phase occupied each element. Our algorithm, as we will discuss in detail shortly, is also different from the extension of Hoshen-Kopelman algorithm by Al-Futaisi and Patzek [144] since we *do not*—except for the first time—scan the *entire* network to update our information regarding the continuity status of different phases residing in every element.

First, the network at its initial condition is scanned to determine continuity of all its present phase locations. Flags are assigned to every single phase location indicating if it is continuous or trapped. If a phase location is trapped then the cluster number which it belongs to is also attached to it. A search algorithm [145] is used to find continuity. The algorithm uses Table IV that lists the circumstances under which phase locations holding the same phase in adjacent pores and throats are considered connected. One should note that we assume that within a single pore or throat all the corners are connected and so are all the layers holding the same phase. This definition of connectivity is used to define clusters of each phase. During the scanning process, if a trapped cluster is found then all phase locations belonging to the cluster are stored under the same cluster number.

TABLE IV. Criteria for connectivity of phase locations holding the same phase in adjacent pores and throats.

Phase location 1[a]	Phase location 2	Connected?
corner	corner	yes
corner	layer	no
corner	center	no
layer	layer	yes
layer	center	yes
center	center	yes

[a]Phase locations 1 and 2 are located in two neighboring elements.

Once the scanning of the network at its initial status is finished, the injection of different phases and thus different displacements may start. Displacements may create new phase locations, form new trapped clusters, and make old trapped clusters break, coalesce, or become continuous. This means that the old flags of phase locations may not be valid anymore and must be updated.

We present a series of displacement-based rules to update the continuity flags after each displacement event. This means that flags will be *always* valid during all processes. Imagine a displacement occurring in a pore or throat. We may call that pore or throat the *target* element which may have several *neighbors*. For a pore, the neighbors are the throats connected to it and for the throats, the pores. Neighbors do not necessarily contain the same fluid as the target element. Every phase location in the target element and its neighbors is considered as a member of a *chain* of phase locations with the same phase and will act as a *head*. If a chain stretches to the inlet and outlet, it is *continuous*, otherwise it is a *trapped* cluster.

The rules are itemized as follows:

1. Before the displacement takes place, all the chain heads in the target element and its neighbors are determined (i.e., *separately* in each pore and throat). For instance, in a corner of an element with configuration group F, see Fig. 7, three chain heads, i.e., water corner, oil layer, and gas center, are determined. One should note that at this stage, there is no need to know how far the chains stretch. Similar phase locations in an element will be members of the same chain and either of them could be used as the chain head. For example, in an element with triangular cross section with all the corners having configuration group G, all the gas layers are considered as members of a gas chain and obviously should all have the same flags and only one of them is used as a chain head. This is also the case for the water corners. However, phase locations with the same phase but in a different *type* of location might not necessarily be considered as members of the same chain. For instance, in configuration group D, water in the center is not considered as a member of the chain that the water corner is a member of, unless they touch each other in a corner where there is no oil layer. The water center is considered as a head of another water chain.

2. Before the displacement, the connectivity of chain heads in the target element with the chain heads in its neigh-

bors are determined and stored using the criteria listed in Table IV.

3. The displacement is carried out which may omit some old phase locations while forming new ones in the target element. Only for the newly formed phase locations must flags be assigned. The new phase locations created by pistonlike, snapoff, and layer formation displacement events that hold *the same* phase as the displacing phase location will get flags exactly the same as those of the displacing phase location. For instance, for oil from the center of a neighbor that creates an oil layer in the target element, the newly formed oil layer will get the same flags as the oil in the center. But if the newly born phase location contains a phase similar to that of the displaced phase location, i.e., old, then it will get the same flags as the displaced phase location. For example, consider configuration group change B to F. The oil layers will get flags the same as those of oil in the center before the displacement.

4. If the displacing phase location is trapped and forms new phase locations with the same flags then the new phase locations are added to the trapped cluster as new members.

5. If the displaced phase location was trapped and after the displacement it does not exist anymore, it is omitted from the list of the trapped cluster members.

6. If the target element is connected directly to the inlet or outlet and the new phase location is formed by the phase invading from the outside of the network, a continuous flag is assigned to the new phase location.

7. After the displacement, new possible chain heads are determined in the target element.

8. Connectivity of the new chain heads in the target elements with the chain heads in the neighbors are determined and stored.

9. Connectivity of every single chain head in the neighbors to the chain heads with the same phase in the target element before and after displacement are compared. If a chain head was disconnected (or connected) to the target element before the displacement and stays disconnected (or connected) after the displacement, there is no need to change the flags of the chain.

10. If a chain head in a neighbor was connected to the target element before the displacement and got disconnected after the displacement then: (i) If the chain head was continuous then its continuity is checked using a search algorithm as the chain might have got trapped due to the disconnection from the target element. (ii) If the chain head was trapped, disconnection from the target element *might* mean that a trapped cluster has *broken* into two or more smaller trapped clusters. This is called a *local break* and the next point describes how the algorithm realizes if a local break has actually broken the displaced trapped cluster into smaller ones.

11. In order to find if a local break is a *break*, one of the phase locations residing in a neighbor that belongs to the displaced (mother) trapped cluster is chosen. Then all the phase locations connected to it are found using a search algorithm. If *all* the other phase locations residing in the neighbor(s) that belong to the mother trapped cluster are among the found phase locations, then the disconnection has been only a local one and not a break. If not, it is a break and the found phase locations form a *new* trapped cluster with a new identity. Now all the other phase locations in the neighbor(s) that were members of the mother trapped cluster are also picked up one by one and all the connected phase locations are found and the process continues exactly the same as for the first phase location until there is no phase location left that has not been assigned to a new smaller trapped cluster.

12. If a chain head in a neighbor was disconnected from the target element before the displacement and has become connected after the displacement then: (i) If the chain in the neighbor was trapped while the chain head in the target element is continuous then the trapped cluster has become continuous and flags of all its members are changed to continuous. The opposite case is also possible when the chain head in the target element is trapped while the one in the neighbor is continuous. (ii) If the chain head in the neighbor was trapped and so was the chain head in the target element that it got connected to, then a *coalescence* has happened and both trapped clusters now will form a bigger trapped cluster (see Sec. VI H 1 for details). For all other cases there is no need to change the flags of the chains.

G. How to choose the right displacement

Based on what phase displaces what phase, there are six possible two-phase processes: oil displacing water which is controlled by an increase in P_{cow}. This could be done either by an increase in oil pressure or a decrease in water pressure. Likewise, water displacing oil (decrease in $P_{cow} \equiv$ increase in water pressure or decrease in oil pressure), gas displacing water (increase in $P_{cgw} \equiv$ increase in gas pressure or decrease in water pressure), water displacing gas (decrease in $P_{cgw} \equiv$ increase in water pressure or decrease in gas pressure), gas displacing oil (increase in $P_{cgo} \equiv$ increase in gas pressure or decrease in oil pressure), and oil displacing gas (decrease in $P_{cgo} \equiv$ increase in oil pressure or decrease in gas pressure). Every displacement belongs to one or two of these six processes. For instance, collapse of the gas layer which leads to configuration group change G to B could occur by either water or oil invasion which corresponds to a decrease in P_{cow} or P_{cgo}, respectively. This means that this displacement belongs to both water displacing gas and oil displacing gas processes. But, for example, configuration group change B to A only belongs to a water displacing oil process.

A process can be carried out either by increasing the pressure of the displacing fluid or decreasing the pressure(s) of the displaced fluid(s). In two-phase processes, both methods may produce the same results but that may *not* necessarily be the case for three-phase systems. We shall model all processes by increasing the pressure of the *injection* fluid. For example, gas injection into water and oil is carried out by increasing the gas pressure not by decreasing the pressures of oil and water.

For every single displacement, a threshold capillary pressure is calculated—Appendix C—which might depend on the relevant contact angles, corner angles and inscribed radius of the element of interest, other capillary pressures, and the configuration of nearest neighbor pores and throats. Then depending on what fluid is displacing and what is displaced,

TABLE V. Multiple displacements search categories (continuous-trapped; c-t).

No.	Displacing fluid	Continuity status	Displaced fluid	Continuity status	Name	Chain categories
1	oil	continuous	water	trapped	ocwt	wtot, wtoc, wtgt, wtgc
2	oil	continuous	gas	trapped	ocgt	gtwt, gtwc, gtot, gtoc
3	gas	continuous	water	trapped	gcwt	wtot, wtoc, wtgt, wtgc
4	gas	continuous	oil	trapped	gcot	otwt, otwc, otgt, otgc
5	water	continuous	oil	trapped	wcot	otwt, otwc, otgt, otgc
6	water	continuous	gas	trapped	wcgt	gtwt, gtwc, gtot, gtoc

the threshold absolute pressure of the *displacing* fluid for a *single* displacement is found from

$$P_i^{threshold} = P_{cij}^{threshold} + P_j \tag{15}$$

or

$$P_j^{threshold} = P_i - P_{cij}^{threshold}, \tag{16}$$

where P_i and P_j are pressures of phases i and j, respectively. The pressure of a fluid is referred to the pressure of a continuous cluster of that fluid and is assumed to be the same as the inlet or outlet pressure of the fluid. There might be several such clusters of one fluid but they all will have the same pressure. The foregoing procedure is used for single displacements where one continuous phase location displaces another continuous one. When one or both of them is trapped, $P_i^{threshold}$ and $P_j^{threshold}$ are found in a slightly different way that shall be discussed in the multiple displacements section (Sec. VII). Threshold pressures of all the displacements that have the same *displacing* fluid are ranked into the same *main sorted list*. Consequently, in three-phase systems there will be three main sorted lists for gas, oil, and water as displacing phases. This means that every list may include entries from two different processes with the same displacing fluid. For instance, the water list may include threshold pressures from water displacing oil and water displacing gas processes.

Initially when the network is water filled, only oil or gas can be injected and the only processes are those that displace water by oil or gas from the elements connected to the inlet. From this stage onwards, new displacements must be added, if there are any, to the appropriate list(s) regardless of whether they could occur during the current process or not. The exact configuration change associated with these new displacements may not be clear at this stage; and it is not necessary, as they may occur during other processes when the conditions, i.e., pressures and target contact angles, will be different. Before a new displacement is added to an appropriate list, its threshold capillary pressure is calculated. Before a new displacement is added to a main sorted list, it must be checked to see if both displacing and displaced phase locations are continuous. If one or both of them is trapped, then the displacement is added into an appropriate *sorted sublist* in one of the 18 multiple displacement search categories tabulated in Tables V–VII [see details in multiple displacements section (Sec. VII)]. If both phase locations are continuous then it is added to an appropriate main sorted list.

By knowing the injection fluid, the relevant main sorted list is selected, for example, the water list for water injection. The list is sorted in ascending order. Imagine the invading fluid is i. This means that we consider a displacement event where the volume of i in an element increases. Phase i can invade either phase j or k. The threshold pressure at the top of the list belongs to the *most favorable*, i.e., easiest, displacement. This could be displacement of j or k by i. If the displacement is *valid* then it takes place. A displacement is valid when the displacing and displaced phase locations are *present* and their continuity status flags are *consistent* with the list that the threshold pressure is in. If a displacement is not valid, the event is taken off the sorted list and either discarded or moved to an appropriate list depending on the reason of invalidity. The next most favorable displacement is considered from the list. The advantage of having one list for both i to j and i to k displacements is that it assures that always the most favorable displacement is carried out *first*.

Displacements in the lists might no longer be valid because of other displacements that have already taken place. For instance, consider configuration group G. Collapse of the gas layer by water in the corner and oil in the center are two possible displacements that should be in the water and oil

TABLE VI. Multiple displacements search categories (trapped-continuous; t-c).

No.	Displacing fluid	Continuity status	Displaced fluid	Continuity status	Name	Chain categories
1	oil	trapped	water	continuous	otwc	
2	oil	trapped	gas	continuous	otgc	
3	gas	trapped	water	continuous	gtwc	
4	gas	trapped	oil	continuous	gtoc	
5	water	trapped	oil	continuous	wtoc	
6	water	trapped	gas	continuous	wtgc	

TABLE VII. Multiple displacements search categories (trapped-trapped; t-t).

No.	Displacing fluid	Continuity status	Displaced fluid	Continuity status	Name	Chain categories
1	oil	trapped	water	trapped	otwt	wtot, wtoc, wtgt, wtgc
2	oil	trapped	gas	trapped	otgt	gtwt, gtwc, gtot, gtoc
3	gas	trapped	water	trapped	gtwt	wtot, wtoc, wtgt, wtgc
4	gas	trapped	oil	trapped	gtot	otwt, otwc, otgt, otgc
5	water	trapped	oil	trapped	wtot	otwt, otwc, otgt, otgc
6	water	trapped	gas	trapped	wtgt	gtwt, gtwc, gtot, gtoc

lists, respectively. If the gas layer collapsed during water invasion by an increase in water pressure, the other displacement, i.e., collapse of the gas layer by oil, is no longer valid as there is no gas layer to be collapsed.

Multiple displacement search categories listed in Tables V–VII allow us to find the most favorable multiple displacement (see later for details), which then is compared with the most favorable single displacement that is determined from the main lists. This comparison would allow us to find the *globally* most favorable event.

After a displacement, the pressure of the phase *i* (injection phase) is set to the *maximum* of the threshold pressure and the current pressure of phase *i*. All the displacements that have threshold pressures less than the pressure of the injection phase *i* are carried out until it is not possible to find a displacement with a threshold pressure less than or equal to the current value of the phase *i* pressure. This is done in a way that the displacement with the *lowest* threshold pressure is ***always*** carried out *first*. At this time, all the configurations are stable and at *equilibrium* and the system is said to be *relaxed*.

The *maximum* of the threshold pressure and the current pressure of phase *i* is used because it is often the case that doing a displacement allows a subsequent displacement at a threshold pressure much lower than the current injection phase pressure. This event is more favorable than the next displacement in the list. An example of this is oil displacement into water in a water-wet medium. P_{oil} may be high to allow oil to fill a throat, but oil can then fill an adjoining pore at a lower oil pressure. If we used this new lower value of P_{oil} to compute radii of curvature, then we would find that in some elements the radius is inconsistent with the fluid configuration—for instance, a water AM in a corner could have a radius of curvature too large to fit in an element. In *strict capillary equilibrium*, the fluid would rearrange throughout the network to give configurations consistent with the prevailing capillary pressure. This is, however, a very difficult task for a general three-phase model. Instead, phase pressures are defined as the maximum value ever reached during the whole simulation. In other words, the pressure of the invading phase *never* acquires a lower value than its current one. Whenever a phase pressure reaches a new maximum, the fluid configurations are truly in a position of capillary equilibrium. In a simulation involving a complex displacement path, the phase pressures will continue to increase. However, since it is only pressure differences that control the displacement sequence, this is not a problem.

As mentioned earlier, threshold capillary pressures may be affected by the change in capillary pressure. In such circumstances, threshold capillary pressures for those displacements are recomputed taking into account the new arrangements of fluid and capillary pressures and re-ordered in the sorted lists. If a new phase is injected then the sorted lists for displacements are re-ordered to account for latest changes in capillary pressures.

H. How to treat trapped clusters, associated radii of curvatures, and displacements

Trapped phases will be in the form of clusters of phase locations. When a cluster of phase locations becomes trapped, (i) A number is assigned to it. (ii) The phase of the cluster is stored. (iii) Addresses of all the phase locations belonging to it are stored. (iv) Two flags are assigned to every single phase location indicating that they are trapped and the the cluster number that they belong to. (v) The current capillary pressures are stored. (vi) The volume of the trapped cluster, which is the summation of volume of its phase locations, when it is trapped is stored as the *original* volume of the cluster. The original volume is used in saturation calculations to account for volume errors caused by multiple displacements (see Sec. IX). (vii) If any of the phase locations of the cluster is involved in a displacement then it is moved to an appropriate sublist in one of the multiple displacement search categories. This could be a move from the main sorted lists to the categories listed in Tables V and VI. If any of the phase locations is involved in displacements that are already in the search categories listed in Tables V and VI, then they need to be moved into corresponding categories in Table VII.

Every multiple displacement search category may contain several sorted sublists. Every sorted sublist within the categories named in Tables V and VI has a cluster number associated with it and contains the threshold pressure of the valid displacements where a trapped cluster can displace continuous fluid or vice versa. Categories listed in Table V contain displacements where the *displaced* phase location is trapped while the categories named in Table VI have the opposite situation. All the sublists are always sorted in ascending order. One should note that the sublists within each category are completely *independent* from each other.

During different three-phase processes, there may be cases where a trapped cluster touches one, two, or several other trapped clusters with different phases. WAG flooding with several injection cycles is an example of such a case. The touching points represent displacements whose threshold pressures are stored in sublists within categories tabu-

lated in Table VII. One trapped cluster might be involved in several sublists as every sublist represents the touching points between only *two* trapped clusters with different fluids. For every sublist, displacing and displaced cluster numbers are also stored.

When a trapped cluster forms, the curvature of all interfaces associated with it need to be kept fixed as long as the cluster is trapped and it has not become involved in multiple displacements. The conventional method in previously developed network models was that the interfaces were considered *frozen*. This was done regardless of the pressure of the phase inside the trapped cluster and pressures of the surrounding fluids. In this work, the pressure of the fluid inside the cluster is *not* a dummy value. It has a physical meaning during the modeling of different processes. The initial pressure of the cluster is the pressure of the phase when it was first trapped. However, the pressure of the cluster changes according to the change in the pressure of the surrounding phases in order to maintain the curvature of the interfaces at the same value as when the trapped cluster first formed. As an example, imagine water flooding into oil in a water-wet system. Trapped clusters of oil form at different stages of water injection, i.e., at different oil-water capillary pressures. Once each trapped cluster forms, it gets the current pressure of oil, i.e., P_{oil}. But since P_{oil} is fixed during water flooding, all the trapped clusters will have the same oil pressure regardless of when they were trapped while the water pressure is increasing. To deal with this problem, we update the pressure of the trapped oil clusters according to the increase in pressure of water using

$$P_{i,new}^{cluster\ k} = P_{cij}^{cluster\ k} + P_{j,new} \tag{17}$$

or

$$P_{j,new}^{cluster\ k} = P_{i,new} - P_{cij}^{cluster\ k}, \tag{18}$$

where $P_{cij}^{cluster\ k} = (P_{i,old}^{cluster\ k} - P_{j,old})$ or $P_{cij}^{cluster\ k} = (P_{i,old} - P_{j,old}^{cluster\ k})$ is the capillary pressure exactly at the moment that the trapped cluster k formed. For the above water flooding example, it becomes

$$P_{oil,new}^{cluster\ k} = (P_{oil,old}^{cluster\ k} - P_{water,old}) + P_{water,new}. \tag{19}$$

The change in pressure of the trapped clusters affects the selection of the most favorable multiple displacement as we shall describe later.

1. Coalescence

During different three-phase processes, trapped clusters may have to move under multiple displacement mechanisms in order to predict a physically correct occupancy. It is quite often the case that the moving trapped clusters meet other trapped clusters of the same phase. This will lead to a *coalescence* event. A coalescence event might also happen when a trapped cluster starts forming layers, if it is possible, between phase locations of the two other phases in the neighboring pores and throats. Layer reformation allows the trapped clusters to extend their margins and meet other trapped clusters. This phenomenon occurs when gas injection is carried out into water flood residual oil in a water-wet system [32,34–36,146]. The merging trapped clusters might have different pressures and volumes, as they might have been trapped at different times during different processes. In such circumstances, we assume that after coalescence the resultant trapped cluster has a *volume weighted* average pressure of the the merging trapped clusters. The *original* volume of the merging trapped clusters may be used in an average pressure calculation as follows:

$$P^{cluster} = \frac{\sum_{k=1}^{n} V_{original}^{cluster\ k} P^{cluster\ k}}{\sum_{k=1}^{n} V_{original}^{cluster\ k}}, \tag{20}$$

where n is the number of merging trapped clusters.

The calculated average pressure of the newly formed trapped cluster is used in saturation calculations and also for multiple displacements. The volume of the trapped cluster formed by coalescence is given by

$$V^{cluster} = \sum_{k=1}^{n} V_{original}^{cluster\ k}. \tag{21}$$

When coalescence happens, all the phase locations of the merging trapped clusters are stored together and are assigned the same cluster number. If there are groups of displacements in categories listed in Tables V and VII that any of the merging clusters were involved in, their threshold pressures are changed according to the new average pressure of the resultant trapped cluster. This is done by

$$P_{i,new}^{threshold} = P_{j,new}^{cluster} + P_{i,old}^{threshold} - P_{j,old}^{cluster\ k} \tag{22}$$

or

$$P_{j,new}^{threshold} = P_{i,new}^{cluster} - P_{i,old}^{cluster\ k} + P_{j,old}^{threshold}. \tag{23}$$

For the displacements in the categories listed in Table VI, threshold pressures are updated if the pressure of the displaced phase which is continuous changes.

In every multiple displacement search category listed in Tables V–VII and all sublists associated with the merging clusters are re-ordered to represent one bigger cluster.

If a trapped cluster meets a continuous cluster of the same phase, the pressure of the *continuous* fluid is changed to that of the trapped cluster if it is greater, otherwise it is left unchanged. All the volume error associated with that trapped cluster is ignored as the system is in contact with the inlet and outlet and the volume error would be compensated automatically. Note that this allows the phase pressures to change due to contact with previously trapped clusters. This method to update pressure is similar to the work of Van Dijke *et al.* [86,87] but different from Fenwick and Blunt [88,89] who kept the continuous cluster pressure constant. All the displacements associated with the trapped cluster are now transferred to the other lists, i.e., main sorted lists or sublists within search categories, as appropriate.

2. When a trapped cluster breaks into smaller ones

In three-phase systems when multiple displacements take place, a trapped cluster might break into two or more smaller ones. For instance, consider an angular element with trapped

oil in the center that is invaded by gas. It is possible that the displaced trapped cluster cannot leave oil layers in the corners of the element and this might disconnect the other phase locations of the displaced trapped cluster that are residing in the neighboring elements. This might also happen, for instance, when an existing layer phase location which is a member of a trapped cluster collapses.

After every multiple displacement, it must be checked if it has caused any break among the phase locations of the displaced trapped cluster(s) residing in neighboring elements. If a break has happened then the number of the resultant smaller clusters and their members are determined and stored using the clustering algorithm described in Sec. VI F.

When a trapped cluster breaks into two or more smaller trapped clusters, the pressure of the smaller clusters are assumed to be *exactly the same* as that of the mother cluster at the time when the break took place. Since the smaller trapped clusters have their own new independent identity, all the displacements associated with the mother trapped cluster in the different multiple displacement search categories must be distributed among the smaller clusters based on which cluster the trapped phase location involved in every displacement is associated with. The original volume of the mother cluster is assigned to the largest of the smaller clusters. The volume of the other clusters is set to zero. This does not create any problems as we shall show in Sec. IX.

VII. MULTIPLE DISPLACEMENTS

One unique feature of three-phase flow at the pore level is multiple displacement. An invasion of phase *j* by phase *i* may be composed of a series of displacements starting with a displacement where *i* is the displacing fluid and ending with a displacement where *j* is the displaced fluid. If all the phases are continuous, this is simply equivalent to separate single displacements. However, the intermediate phases in the chain may be trapped. This means that a cascade of trapped clusters nudge each other before a final displacement of a continuous phase. Trapped clusters of the intermediate phases can rearrange themselves in the pore space and/or reform layers, and may coalesce with other trapped clusters of the same phase to make bigger trapped clusters or become continuous by meeting continuous clusters. This happens simply due to capillary forces. Multiple displacements that involve more than one intermediate stage are only possible if there are trapped clusters of at least two phases [87]. If only one phase has any trapped clusters, a simpler version of multiple displacement, *double displacement*, may take place and this has been observed in micromodel experiments [35,40,43,136] and coded into network models [87–89,112], where one phase invades part of a trapped cluster that in turn displaces the third continuous phase.

Here we present a search algorithm that is capable of finding the most favorable multiple displacement. In this work, we use it to find the most favorable double displacement only. During each process, the most favorable double displacement is compared with the most favorable single displacement. The one that requires the lower pressure of the injection phase is the one that takes place. In order to find the most favorable double displacement, all the possible double events for all the trapped clusters in the system need to be considered.

The algorithm for considering such events is somewhat involved, since multiple events for all clusters need to be considered [87]. Here we present how the most favorable multiple displacement is found every time.

First, based on what fluid is being injected into the system, the two categories from Table V that have the same displacing fluid as the injection fluid are considered and called *starting* categories. For instance, categories *gcwt* and *gcot* are considered (*c* indicates continuous and *t* trapped) when gas is being injected. Now all the categories that could chain up with the starting categories are determined from Tables V and VII and are called *chain categories*. Chain categories for *gcwt* and *gcot* would be *wtot*, *wtoc*, *wtgt*, *wtgc*, *otwt*, *otwc*, *otgt*, and *otgc*. As mentioned earlier, every category might include several sublists with one or two trapped cluster numbers associated with each one. The displacements at the top of each sublist within the starting categories can now chain up with the displacements at the top of the sublists within the chain categories, if there are any, provided that the displacing trapped cluster number of the sublist within the chain category is the *same* as the displaced trapped cluster number of the sublist within the starting category. This means that every trapped cluster involved in a multiple displacement contributes to two displacements. The displaced phase of a category must be the same as the displacing phase of the category that it is going to chain up with. The displacement at the top of each sublist is the easiest, i.e., lowest invasion pressure, displacement of the sublist. So every multiple displacement is a chain of easiest displacements from sublists within categories that are allowed to chain up with each other. Chaining up with categories continues until the next category is one of those tabulated in Table VI. For example, the chain of *gcot*, *otwt*, *wtgt*, and *gtwc* could give multiple displacements provided that sublists satisfying the foregoing conditions exist within the above categories. This in turn means that oil, water, and gas trapped clusters existed in the system. Continuous gas touches trapped oil clusters which in turn touch trapped water clusters which in turn touch trapped gas clusters which in turn touch continuous water. For a multiple displacement with *n* trapped clusters involved, a series of $n+1$ chainlike displacements are carried out. Using the foregoing algorithm, all the possible multiple displacements are determined and their threshold absolute pressure are calculated using

$$P_{i,MD}^{threshold} = \sum_{k=1}^{n} \left[\left(P_j^{threshold}\right)^{cluster\ k} - P_{j,old}^{cluster\ k} \right] + P_i^{threshold}, \tag{24}$$

where *n* is the number of trapped clusters involved, MD stands for multiple displacement, $P_i^{threshold}$ is the threshold pressure of the first displacement of the multiple displacement where the injection fluid is the displacing fluid, *j* is the fluid that cluster *k* accommodates, $\left(P_j^{threshold}\right)^{cluster\ k}$ is the threshold absolute pressure of the displacement for which trapped cluster *k* is the *displacing* fluid, and $P_{j,old}^{cluster\ k}$ is the

old pressure of the trapped cluster *k*, i.e., before the multiple displacement. Equation (24) has been derived by summing up the threshold capillary pressures of all the displacements. One should note that the threshold capillary pressure of each displacement in a multiple displacement is calculated using a contact angle that is defined according to what fluid is displacing what, *regardless* of what fluid is being injected into the system. When a multiple displacement is carried out pressures of the involved trapped clusters are increased to the value given by

$$P_{j,new}^{cluster\ k} = (P_j^{threshold})^{cluster\ k}. \quad (25)$$

We give an example of applying this algorithm by considering a double displacement which is used in this work. Imagine gas is being injected into oil and water where some of the oil is in trapped clusters. Since there are only trapped oil clusters the only possible multiple displacement is double displacement where continuous gas displaces trapped oil which in turn displaces continuous water. The double displacements are determined by chaining up categories *gcot* and *otwc*. The threshold capillary pressure of the double displacement is

$$P_{\mathrm{gas},DD}^{threshold} = P_{gas}^{threshold} + [(P_{oil}^{threshold})^{cluster} - P_{oil,old}^{cluster}], \quad (26)$$

where DD stands for double displacement. The new pressure of the trapped oil cluster is

$$P_{oil,new}^{cluster} = (P_{oil}^{threshold})^{cluster}. \quad (27)$$

Once a multiple displacement is recognized as a *global* most favorable event, it is carried out. But there is one subtlety involved. It is quite often the case that $P_{i,MD}^{threshold}$ is smaller than P_i. In other words, the multiple displacement could be carried out without any increase in pressure of phase *i*. The difference between these two pressures needs to be accounted for in the pressures of trapped clusters involved in multiple displacement by increasing them by $(P_i - P_{i,MD}^{threshold})$.

To calculate the threshold pressure of a multiple displacement, one may use threshold pressures of the displacements involved regardless of their type. This means that displacements may well be layer formation or collapse events. Theoretically this is fine but not *technically*. (i) This approach might increase the volume error associated with multiple displacement as pistonlike, pore-body filling, and snapoff events might chain up with the layer formation or collapse events which would obviously be detrimental for volume conservation. (ii) The simulator might be trapped in an infinite loop of forming and collapsing layers. To prevent these problems, we shall use a slightly different approach where only threshold pressures of pistonlike, pore-body filling, and snapoff events are used in calculating the threshold pressure of a multiple displacement. When a multiple displacement is to be carried out, all the layer formation or collapse events in the involved sublists that are *more favorable* to the displacements used in $P_{i,MD}^{threshold}$ calculations, are carried out *first*.

As we mentioned earlier, when a multiple displacement is taking place, the pressures of the involved trapped clusters increase. Once this happens, we then *update all* the AM's associated with the trapped clusters according to their new pressures. This means that the volumes of the trapped clusters are always kept updated. Also the *new* AM's formed during the multiple displacements will have radii of curvatures according to the new pressures of the trapped clusters that they belong to.

After every multiple displacement event, new displacements that are now available have to be added to the sublists within the correct categories. This means that we might have new chains of displacements, i.e., multiple displacements, for the next round. Also there might be phase locations that must be added to or omitted from the involved trapped cluster(s). For example, imagine that a trapped gas cluster is to displace trapped oil in the center of a triangular throat. Before the displacement, configurations in all the corners are from group *B* and the center phase location is a member of a trapped oil cluster. Also imagine that corner half angles, contact angles, and capillary pressures allow oil to reside as a layer in at least one corner after the oil in the center is displaced by gas. After the displacement, the configurations in two corners are changed to C and in one corner to F. Once the configurations are changed, the center phase location must be omitted from the trapped oil cluster and added to the trapped gas cluster as it now accommodates gas. Also one oil layer phase location residing in one of the corners must be added to the displaced trapped oil cluster. The new displacements that must be added to the appropriate lists are: oil layer collapse by water in the corner to be added into the *right* sublist, i.e., the sublist with the same cluster number, within the *wcot* category provided that water in the corner is continuous, oil layer collapse by gas in the center to be added into the right sublist within the *gtot* category, snapoff of the gas in the center by oil layer to be added into the right sublist within the *otgt* category, snapoff of gas in the center by water in the corners to be added into the right sublist within the *wcgt* category, and other displacements in connection with continuous and trapped fluids residing in the neighboring elements.

VIII. SATURATION PATH TRACKING

As discussed in the literature review, macroscopic properties in three-phase systems are strongly dependent on the saturation history of the system. This means that prediction of experimental measurements is possible only if the experimental saturation history is reproduced by the model. We track the experimental saturation paths on a point by point basis.

Every given saturation path is composed of a series of points in saturation space. The first saturation target (of oil, water, and gas) is specified. The difference between the present saturations and the target saturations are found. The phase with the most *negative* difference is the next to be injected. Imagine that is phase *i*. This means that we consider a displacement where the volume of *i* in an element increases. Injection of phase *i* continues until the difference between the present and the target saturation of phase *i* is not the most negative difference. Another phase with the most negative difference is then injected. This continues until the

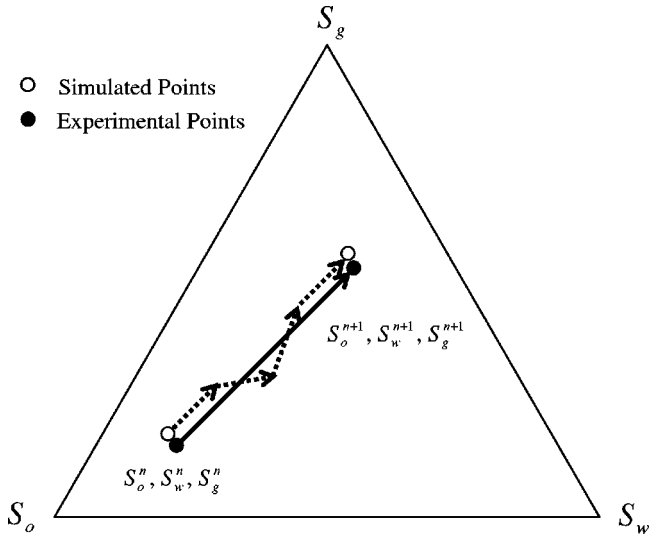

FIG. 13. Schematic presentation of the saturation tracking method.

saturation differences fall within a predefined tolerance. Then a new saturation target is considered. This process continues until the desired saturation path is produced; see Fig. 13.

Tracking an experimental path using a network model is practically very complex and difficult. This is because of finite size effects, the percolation nature of the processes, and hysteresis. For instance, in some cases during a saturation tracking procedure, the system does not *relax* before several thousand displacements have been performed which will take the saturations far away from the desired path. However, in the cases we present in this work, this does not significantly affect the results.

IX. COMPUTATION OF SATURATION, CAPILLARY PRESSURE, AND RELATIVE PERMEABILITY

Saturation, capillary pressure, and relative permeability are only computed when the phase pressure reaches a new maximum—this means that the system is at equilibrium and it is not possible to carry out any displacements with the current phase pressures. The capillary pressure is found from the pressure difference between continuous phases. If V_p^i is the volume of phase p in element i (including the water volume in clay) then the saturation of phase p is given by

$$S_p = \frac{\sum_{i=1}^{n_e} V_p^i + V_p^{error}}{\sum_{j=1}^{n_p} \sum_{i=1}^{n_e} V_j^i + \sum_{j=1}^{n_p} V_j^{error}}, \tag{28}$$

where n_p is the number of phases, n_e is the total number of pores and throats, and V_p^{error} is the volume error of phase p caused by multiple displacements and is given by

$$V_p^{error} = \sum_{i=1}^{n_p^c} (V_p^{original} - V_p^{present})_i, \tag{29}$$

where n_p^c is the number of trapped clusters of phase p. The total volume, inscribed radius, and shape of each element are read in as input data. The volume of a phase in an element is the total volume multiplied by the fraction of the cross-sectional area occupied by that phase. Saturation is computed within a selected region, i.e., between inlet and outlet surfaces of the network rather than over the whole network (Appendix B). Expressions used to compute areas are given in Appendix A. The procedure to compute conductance, absolute, and relative permeability is given in Appendix B.

X. CONCLUSIONS

A definitive capillary dominated three-phase network model was developed that combines three essential components: (i) a description of the pore space and its connectivity that mimics *real* systems; (ii) a physically based model of *wettability alteration*; (iii) a *full description of fluid configurations* for two- and three-phase flow.

The model can accommodate any combination of oil-water, gas-water, and gas-oil contact angles and uses a robust clustering algorithm to account for trapping and double displacement.

ACKNOWLEDGMENTS

The members of the Imperial College Consortium on Pore-Scale Modeling (BHP, Enterprise, Gaz de France, JNOC, PDVSA-Intevep, Schlumberger, Shell, Statoil, the U.K. Department of Trade and Industry, and the EPSRC) are thanked for their financial support. We also thank Pål-Eric Øren (Statoil) for sharing his Berea network data with us and also his valuable comments. We thank Gary Jerauld (BP) for providing the Oak data in electronic form and Ken Sorbie (Heriot-Watt University) for his insightful comments on this work.

APPENDIX A: AREA OPEN TO FLOW

The equations used to compute the total area of a pore or throat with different cross sections are

$$A_t = \pi R^2, \quad \text{circular cross section}, \tag{A1}$$

$$A_t = 4R^2, \quad \text{square cross section}, \tag{A2}$$

$$A_t = \frac{R^2}{4G}, \quad \text{triangular cross section}, \tag{A3}$$

where R and G are the inscribed radius and shape factor of the pore or throat, respectively.

The corner area open to flow is calculated using

$$A_c = r^2\left(\cos\theta(\cot\alpha\cos\theta - \sin\theta) + \theta + \alpha - \frac{\pi}{2}\right), \tag{A4}$$

$$A_c = \left(r\frac{\cos(\theta+\alpha)}{\sin\alpha}\right)^2 \sin\alpha\cos\alpha \quad \text{if } \alpha+\theta = \frac{\pi}{2}, \tag{A5}$$

where r is the radius of curvature which corresponds to the ratio of interfacial tension to the capillary pressure of the interface, α is the corner half angle, and θ is the angle that

the interface makes with the solid surface towards the corner that is not necessarily the contact angle of the interface, e.g., θ_I and θ_{II} in Fig. 14.

If a layer is present in the corner, the layer area is the total area of the corner including the layer minus the corner area excluding the layer and both are calculated using Eqs. (A4) and (A5) but with pertinent r and θ. For instance, in configuration group F, first the total corner area, $A_c = A_{w\ corner} + A_{o\ layer}$, is calculated with r and θ of the gas-oil interface and then $A_{w\ corner}$ is found using r and θ of the oil-water interface. Then $A_{o\ layer} = A_c - A_{w\ corner}$. The same procedure is used to calculate the area of the the second layer, if present. The area open to flow to a phase in the center of an angular element is the total area of the element minus the summation of the corner areas, including the layers (if present).

APPENDIX B: CONDUCTANCES—ABSOLUTE AND RELATIVE PERMEABILITIES

When saturation is computed, relative permeability and capillary pressure can also be found. This is not done after every saturation computation to save computer time. Typically, relative permeability is calculated around 20–40 times during a simulation. To compute absolute and relative permeability, conductances of each continuous phase location in each element are first computed. Normally exact analytic results are not possible, and empirical expressions derived from solutions of the Stoke's equation for flow in pores of different geometries and for different fluid configurations are used [47–49,67,132,138,147]. Then the average conductance for each phase in the whole network is computed by explicitly calculating the flow through the network assuming conservation of volume. From this absolute and relative permeability can be found [48,67,89,148].

In order to minimize end effects on calculated macroscopic properties, we calculate saturation within two surfaces perpendicular to the main flow direction bounding the central 90% of the network. However, the pressure is solved over whole network to find the pressure in each pore. The pressure of the fluid whose permeability is being calculated is found at the two surfaces by

$$P_a = \frac{\sum_{i=1}^{n} P_a^i A_a^i}{\sum_{i=1}^{n} A_a^i}, \tag{B1}$$

where P_a is the pressure of phase a at the surface, P_a^i is the pressure of phase a in a pore or throat at the point that touches the surface, A_a^i is the area open to flow for phase a through that pore or throat, and n is the number of pores and throats touching the surface. When the element that touches the surface is a pore then the pressure of the phase a at the touching point will be the pore pressure of fluid a and is known after the pressure is solved over the whole network. But if it is a throat, then the pressure at the touching point is found by a linear interpolation between the pressures of phase a in two connecting pores located in two sides of the surface. This is similar to the procedure used by Øren *et al.* [48].

The absolute permeability of the network is calculated using Darcy's law:

$$K = \frac{\mu_a Q_a^{total} L}{A \Delta P}, \tag{B2}$$

where K is the absolute permeability, μ_a the viscosity of fluid a, L is the distance, and ΔP is the corresponding pressure drop between the vertical surfaces. A is the cross-sectional area perpendicular to the main direction of flow, Q_a^{total} is the total flow rate of fluid a.

First it is assumed that the network is completely filled with only one phase a. Conductance is calculated using the following equations [48,149]:

$$g = \frac{0.5GA^2}{\mu}, \quad \text{circular cross section}, \tag{B3}$$

$$g = \frac{0.5623GA^2}{\mu}, \quad \text{square cross section}, \tag{B4}$$

$$g = \frac{3R^2A}{20\mu}, \quad \text{triangular cross sections}. \tag{B5}$$

The conductance of a phase a, through an assembly of two pores connected to each other by a throat, is considered to be the *harmonic* mean of the conductance to the phase through the pores and the connecting throat [89]:

$$\frac{L_{ij}}{g_{ij}^a} = \frac{L_{t_{ij}}}{g_{t_{ij}}^a} + \frac{L_{p_{ij}}}{g_{p_i}^a} + \frac{L_{p_{ji}}}{g_{p_j}^a}, \tag{B6}$$

where L_{ij} is the distance between the centers of two connected pores, g_{ij}^a is the conductance of the assembly to phase a, $L_{t_{ij}}$ is the throat length, $g_{t_{ij}}^a$ the throat conductance to phase a, $L_{p_{ij}}$ and $L_{p_{ji}}$ are the half length of the pores, and $g_{p_i}^a$ and $g_{p_j}^a$ are conductance of the pores i and j to phase a, respectively.

The flow rate of the phase between two connected pores, i.e., q_{ij}^a is then given by [89]

$$q_{ij}^a = \frac{g_{ij}^a}{L_{ij}} (P_{p_i}^a - P_{p_j}^a), \tag{B7}$$

where $P_{p_i}^a$ and $P_{p_j}^a$ are the pressures of fluid a in pores i and j, respectively.

Conserving volume for fluid a in each pore gives

$$\sum_{i=1}^{m_i} q_{ij}^a = 0, \tag{B8}$$

where m_i is the number of connected throat pores containing continuous phase a. If Eq. (B6) is written for all such throat pores and then inserted into Eq. (B8), a system of linear equations is formed for the pore pressures that is solved using the *conjugate gradient* method [48]. Having the pore pressures allows us to calculate the total flow rate of the phase, i.e., Q_{total}^a, which in turn is used in Eq. (B2) to calculate the absolute permeability of the network, K.

Relative permeabilities are computed only when the network contains more than one phase. They are calculated only

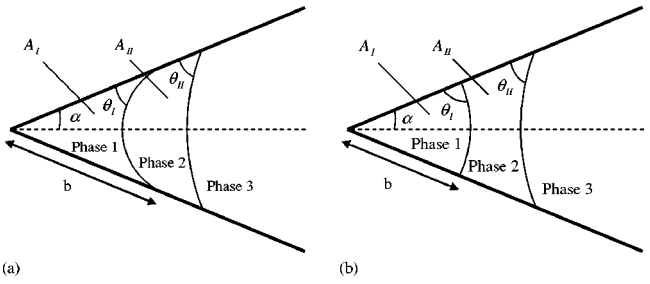

FIG. 14. Corners with a sandwiched layer, (a) first interface has a positive curvature, (b) first interface has a negative curvature.

for phases that have at least one network-spanning cluster (a cluster that is continuous from inlet to outlet).

First the conductance in all the pore and throats containing continuous phase a is computed. Then using the same procedure used for the calculation of absolute permeability, the pressures of the phase in the pores that are a member of spanning cluster(s) are found using the same pressure drop across the network as used for single-phase flow. The relative permeability is

$$k_r^a = \frac{Q_{total}^a}{Q_{total}^{single\ phase}}. \tag{B9}$$

When a network has elements with noncircular cross section, a single element might accommodate up to three fluids in it. A fluid, as it was shown in Figs. 6 and 7, might be residing in corners, layers, or the center of a noncircular element. For the fluid in the center of an element, Eqs. (B3)–(B5) are still used to find the conductance with A being only the area open to flow to the fluid at the center.

Several authors have proposed expressions to compute the conductance of layers [30,39,91,132,150–152]. In this work, we use the expressions proposed by Hui and Blunt [132] to compute the conductance of wetting and spreading layers. When $\theta_I \leqslant \pi/2-\alpha$, see Fig. 14(a), the conductance of the element to the phase flowing in the corner can be estimated by

$$g = \frac{A_c^2(1-\sin\alpha)^2(\varphi_2\cos\theta-\varphi_1)\varphi_3^2}{12\mu\sin^2\alpha(1-\varphi_3)^2(\varphi_2+f\varphi_1)^2}, \tag{B10}$$

$$\varphi_1 = \left(\frac{\pi}{2}-\alpha-\theta\right), \tag{B11}$$

$$\varphi_2 = \cot\alpha\cos\theta-\sin\theta, \tag{B12}$$

$$\varphi_3 = \left(\frac{\pi}{2}-\alpha\right)\tan\alpha, \tag{B13}$$

where $\theta=\theta_I$, $A_c=A_I$, $f=1$ for a no-flow boundary condition suitable for oil-water interfaces, and $f=0$ when a free boundary condition is applied for gas-oil or gas-water interfaces.

If $\theta_I > \pi/2-\alpha$, see Fig. 14(b), the corner conductance is calculated using

$$g = \frac{A_c^2\tan\alpha(1-\sin\alpha)^2\varphi_3^2}{12\mu\sin^2\alpha(1-\varphi_3)(1+f\varphi_3)^2}. \tag{B14}$$

When there is a fluid layer sandwiched between the phases residing in the corner and center, corner and layer, or layer and center (see Figs. 6 and 7), the conductance of the element to the sandwiched phase can be estimated by

$$g = \frac{A_1^3(1-\sin\alpha)^2\tan\alpha\varphi_3^2}{12\mu A_c\sin^2\alpha(1-\varphi_3)\left[1+f_1\varphi_3-(1-f_2\varphi_3)\sqrt{\frac{A_2}{A_c}}\right]^2}, \tag{B15}$$

where A_1 is the area of the layer that the conductance is being calculated for, A_c is a summation of areas of corner and layer (if present) above the layer of interest, and $A_2=A_c-A_1$. For instance, to calculate the conductance of the gas layer in configuration group J, see Fig. 7, $A_1=A_{g\ layer}$, $A_c=A_{w\ corner}+A_{o\ layer}+A_{g\ layer}$, and $A_2=A_{w\ corner}+A_{o\ layer}$. The corner and layer areas are calculated using Eqs. (A4) and (A5).

APPENDIX C: THRESHOLD CAPILLARY PRESSURES

The equations used to compute threshold capillary pressures for all displacements described in Sec. VI D are presented here [27,48,67,148]. Tables VIII–XIV name the equations used in different process with different range of contact angles.

Equations (C1)–(C18) are used to calculate threshold capillary pressures of pistonlike displacements, see Tables VIII–XI to find which equation is used for what range of contact angles. The tables also provide information on θ_1, θ_2, and θ for each case (if required).

$$P_c = \frac{\sigma(1+2\sqrt{\pi G})\cos\theta_1}{R}F_d(\theta_2,G,E), \tag{C1}$$

where σ is the interfacial tension, R the inscribed radius, and G the shape factor.

$$F_d(\theta_2,G,E) = \frac{1+\sqrt{1-[(4GE)/\cos^2\theta_2]}}{1+2\sqrt{\pi G}}, \tag{C2}$$

$$E = \sum_{i=1}^{3}\cos\theta_2\frac{\cos(\theta_2+\alpha_i)}{\sin\alpha_i}-\left(\frac{\pi}{2}-\theta_2-\alpha_i\right), \tag{C3}$$

where α is the corner half angle.

$$P_c = \frac{2\sigma\cos\theta}{R}. \tag{C4}$$

Note in the following equations, $\alpha_1 \leqslant \alpha_2 \leqslant \alpha_3$ for a triangular cross section:

$$b_i = r_{extreme}\frac{\cos(\theta_1+\alpha_i)}{\sin\alpha_i}, \tag{C5}$$

$$r_{extreme} = \frac{\sigma}{P_{c,extreme}}, \tag{C6}$$

if the interface has not moved yet. The $P_{c,extreme}$ belongs to the last move of the interface. If the interface has moved,

TABLE VIII. Threshold capillary pressure for pistonlike and pore-body filling displacements with layers of the invading phase contributing to the displacement—oil to water, gas to water, and gas to oil.

Cross section	Contact angle range	Equation(s)	θ_1[a]	θ_2	θ	Comment
Triangular	$\theta_{ij} < \pi/2 - \alpha_1$[b]	(C1)–(C3)	θ_{ij}[c]	θ_{ij}		
Triangular	$\theta_{ij} < \theta_{extreme}$[d] and $\theta_{ij} \geqslant \pi/2 - \alpha_1$	(C4)			θ_{ij}	
Triangular	$\theta_{ij} \geqslant \theta_{extreme}$ and $\theta_{ij} \geqslant \pi/2 - \alpha_1$	[throats (C5)–(C12) and (C14)], [pores (C19)]	[e]	$\pi - \theta_{ij}$	θ_{ij}	iterative
Square	$\theta_{ij} < \pi/4$	(C15)		θ_{ij}		
Square	$\theta_{ij} < \theta_{extreme}$ and $\theta_{ij} \geqslant \pi/4$	(C4)			θ_{ij}	
Square	$\theta_{ij} \geqslant \theta_{extreme}$ and $\theta_{ij} \geqslant \pi/4$	[throats (C5)–(C13)], [pores (C19)]	[e]	$\pi - \theta_{ij}$	θ_{ij}	iterative
Circular	$0 \leqslant \theta_{ij} \leqslant \pi$	(C4)			θ_{ij}	

[a]Contact angle that interface moved with last time.
[b]Half angle of the sharpest corner.
[c]$\theta_{ij} = \theta^r_{ij}$, $ij = ow, go, gw$—$\theta_{ow} = \theta^{PD}_{ow}$, and $\theta_{gw} = \theta^{PD}_{gw}$ for displacement of water by gas and oil during primary drainage.
[d]$\theta_{extreme} = \pi - \theta_3$, where θ_3 is calculated using Eqs. (C17) and (C18) for triangular and square cross sections, respectively.
[e]It can be either $\pi - \theta_1$ or θ_1 based on the type of AM that θ_1 belongs to. It is the angle that the AM makes with the surface towards the apex of the corner.

$$b_i = r_p \frac{\cos(\theta_2 + \alpha_i)}{\sin \alpha_i}, \tag{C7}$$

$$\theta_i^h = \cos^{-1}\left(\frac{r_{extreme}}{r_p} \cos(\theta_1 + \alpha_i) \right) - \alpha_i \tag{C8}$$

if the interface has not moved yet. If the interface has moved,

$$\theta_i^h = \theta_2, \tag{C9}$$

$$a_i = \sin^{-1}\left(\frac{b_i \sin \alpha_i}{r_p} \right) \tag{C10}$$

if the interface has not moved yet. If the interface has moved,

$$a_i = \frac{\pi}{2} - \theta_2 - \alpha_i, \tag{C11}$$

$$P_c = \frac{\sigma}{r_p}, \tag{C12}$$

$$r_p = \frac{R^2 - r_p b \cos \theta^h + r_p^2 \left(\frac{\pi}{2} - \theta^h - \alpha \right)}{2 r_p a + 2[R - b] \cos \theta_2}, \tag{C13}$$

$$r_p = \frac{\frac{R^2}{4G} - r_p \sum_{i=1}^{n} b_i \cos \theta_i^h + r_p^2 \sum_{i=1}^{n} \left(\frac{\pi}{2} - \theta_i^h - \alpha_i \right) - A}{2 r_p \sum_{i=1}^{n} a_i + \left[\frac{R}{2G} - 2 \sum_{i=1}^{3} b_i \right] \cos \theta_2}. \tag{C14}$$

n = number of contributing corners, A = summation of corner areas (only those corners that do not have layers or corners of the invading phase).

$$P_c = \frac{\sigma}{R} \left[\cos \theta_2 + \sqrt{\frac{\tan \alpha}{2} (\sin 2\theta_2 - 2\theta_2 - 2\alpha + \pi)} \right], \tag{C15}$$

$$P_c = \frac{\sigma}{R} \left[\cos \theta_2 - \sqrt{\frac{\tan \alpha}{2} (-\sin 2\theta_2 + 2\theta_2 - 2\alpha - \pi)} \right], \tag{C16}$$

$$\theta_3 = \cos^{-1}\left(\frac{-2 r_{extreme} \sum_{i=1}^{n} a_i}{\frac{R}{2G} - 2 \sum_{i=1}^{3} b_i} \right), \tag{C17}$$

n = number of corners containing layers or filled corners of the invading phase.

TABLE IX. Threshold capillary pressure for pistonlike and pore-body filling displacements with *no* layers of the invading phase contributing to the displacement—oil to water, gas to water, and gas to oil.

Cross section	Contact angle range	Equation(s)	θ_1[a]	θ_2	θ	Comment
Triangular	$\theta_{ij} < \pi/2 - \alpha_1$	(C1)–(C3)	θ_{ij}	θ_{ij}		
Triangular	$\theta_{ij} \geqslant \pi/2 - \alpha_1$	(C4)			θ_{ij}	
Square	$\theta_{ij} < \pi/4$	(C15)		θ_{ij}		
Square	$\theta_{ij} \geqslant \pi/4$	(C4)			θ_{ij}	

[a]Contact angle that interface moved with last time.

TABLE X. Threshold capillary pressure for pistonlike and pore-body filling displacements with layers of the invading phase contributing to the displacement—water to oil, water to gas, and oil to gas.

Cross section	Contact angle range	Equation(s)	θ_1[a]	θ_2	θ	Comment
Triangular	$\theta_{ij} > \pi/2 + \alpha_1$[b]	(C1)–(C3)	θ_{ij}[c]	$\pi - \theta_{ij}$		
Triangular	$\theta_{ij} \geqslant \theta_{extreme}$[d] and $\theta_{ij} \leqslant \pi/2 + \alpha_1$	(C4)			θ_{ij}	
Triangular	$\theta_{ij} < \theta_{extreme}$ and $\theta_{ij} \leqslant \pi/2 + \alpha_1$	[throats (C5)–(C12) and (C14)], [pores (C19)]	[e]	θ_{ij}	θ_{ij}	iterative
Square	$\theta_{ij} > 3\pi/4$	(C16)		θ_{ij}		
Square	$\theta_{ij} \geqslant \theta_{extreme}$ and $\theta_{ij} \leqslant 3\pi/4$	(C4)			θ_{ij}	
Square	$\theta_{ij} < \theta_{extreme}$	[throats (C5)–(C13)], [pores (C19)]	[e]	θ_{ij}	θ_{ij}	iterative
Circular	$0 \leqslant \theta_{ij} \leqslant \pi$	(C4)			θ_{ij}	

[a]Contact angle that interface moved with last time.
[b]Half angle of the sharpest corner.
[c]$\theta_{ij} = \theta^a_{ij}$, $ij = ow, go, gw$.
[d]$\theta_{extreme} = \theta_3$, where θ_3 is calculated using Eqs. (C17) and (C18) for triangular and square cross sections, respectively.
[e]It can be either $\pi - \theta_1$ or θ_1 based on the type of AM that θ_1 belongs to. It is the angle that the AM makes with the surface towards the apex of the corner.

$$\theta_3 = \cos^{-1}\left(\frac{-r_{extreme}a}{R-b}\right). \tag{C18}$$

For pore-body filling we use Eq. (C19) [148]. See Tables VIII and X for the range of contact angles in which this equation is used.

$$P_c = \frac{2\sigma\cos\theta}{R_p} - \sigma\sum_{i=1}^{n} e_i x_i, \tag{C19}$$

where n is the number of throats that *do not* contribute to the invasion of the bore body, $R_{t,i}$ are the inscribed radii of the such throats, x_i are random numbers, R_p is inscribed radius of the pore, and e_i are predefined parameters. For instance, imagine an oil filled water-wet circular cross-section pore with eight throats connected to it. If two of the throats contain oil in the center, two gas, one trapped water, and only three continuous water, then for the water invasion of the pore: $n=2+2+1=5$. In this work, we use Eq. (C19) with $e_1=0$ and $e_2-e_n=0.03\ \mu\text{m}^{-1}$ [70,148].

Equations (C20)–(C34) are used for snapoff. Tables XII and XIII list the equations that are used for different ranges of contact angles in elements with triangular and square cross sections,

$$P_c = \frac{\sigma}{R}\left(\cos\theta_2 - \frac{2\sin\theta_2}{\cot\alpha_1 + \cot\alpha_2}\right), \tag{C20}$$

$$P_c = \frac{\sigma(\cot\alpha_1\cos\theta_2 - \sin\theta_2)}{R(\cot\alpha_1 + \cot\alpha_2) - b_2}, \tag{C21}$$

$$P_c = \frac{\sigma}{R}\left(\cos\theta_2 - \frac{2\sin\theta_2}{\cot\alpha_1 + \cot\alpha_3}\right), \tag{C22}$$

$$P_c = \frac{\sigma(\cot\alpha_1\cos\theta_2 - \sin\theta_2)}{R(\cot\alpha_1 + \cot\alpha_3) - b_3}, \tag{C23}$$

$$P_c = \frac{\sigma}{R}\left(\cos\theta_2 - \frac{2\sin\theta_2}{\cot\alpha_2 + \cot\alpha_3}\right), \tag{C24}$$

$$P_c = \frac{\sigma(\cot\alpha_2\cos\theta_2 - \sin\theta_2)}{R(\cot\alpha_2 + \cot\alpha_3) - b_3}. \tag{C25}$$

If only one corner has a contributing AM, we *assume* that the element is filled when the AM moves and meets a *noncontributing* AM at one of the other corners.

$$P_c = \frac{\sigma(\cot\alpha_1\cos\theta_2 - \sin\theta_2)}{R(\cot\alpha_1 + \cot\alpha_3)} \tag{C26}$$

if only corner 1 has a layer or filled corner of the invading phase.

TABLE XI. Threshold capillary pressure for pistonlike and pore-body filling displacements with *no* layers of the invading phase contributing to the displacement—water to oil, water to gas, and oil to gas.

Cross section	Contact angle range	Equation(s)	θ_1[a]	θ_2	θ	Comment
Triangular	$\theta_{ij} > \pi/2 + \alpha_1$	(C1)–(C3)	θ_{ij}	$\pi - \theta_{ij}$		
Triangular	$\theta_{ij} \leqslant \pi/2 + \alpha_1$	(C4)			θ_{ij}	
Square	$\theta_{ij} > 3\pi/4$	(C16)		θ_{ij}		
Square	$\theta_{ij} \leqslant 3\pi/4$	(C4)			θ_{ij}	

[a]Contact angle that interface moved with last time.

TABLE XII. Threshold capillary pressure for snap-off displacements—oil to water, gas to water and gas to oil.

Cross section	Contact angle range	Equation(s)	θ_1[a]	θ_2	Comment
Triangular	$\theta_{ij} \geq \pi/2 + \alpha_1$	(C20)–(C31)		$\pi - \theta_{ij}$	min P_{cij}
Triangular	$\theta_{ij} \geq \alpha_1$ and $\theta_{ij} \leq \pi/2 + \alpha_1$	(C32)	[b]	$\pi - \theta_{ij}$	
Triangular	$\theta_{ij} < \alpha_1$	(C33)	[b]	$\pi - \theta_{ij}$	
Square	$\theta_{ij} > 3\pi/4$	(C34)		$\pi - \theta_{ij}$	
Square	$\theta_{ij} \geq \pi/4$ and $\theta_{ij} \leq 3\pi/4$	(C32)	[b]	$\pi - \theta_{ij}$	
Square	$\theta_{ij} < \pi/4$	(C33)	[b]	$\pi - \theta_{ij}$	

[a]Contact angle that interface moved with last time.
[b]It can be either $\pi - \theta_1$ or θ_1 based on the type of AM that θ_1 belongs to. It is the angle that the AM makes with the surface towards the apex of the corner.

$$P_c = \frac{\sigma(\cot \alpha_1 \cos \theta_2 - \sin \theta_2)}{R(\cot \alpha_1 + \cot \alpha_2)} \tag{C27}$$

if only corner 1 has a layer or filled corner of the invading phase.

$$P_c = \frac{\sigma(\cot \alpha_2 \cos \theta_2 - \sin \theta_2)}{R(\cot \alpha_2 + \cot \alpha_3)} \tag{C28}$$

if only corner 2 has a layer or filled corner of the invading phase.

$$P_c = \frac{\sigma(\cot \alpha_2 \cos \theta_2 - \sin \theta_2)}{R(\cot \alpha_2 + \cot \alpha_1)} \tag{C29}$$

if only corner 2 has a layer or filled corner of the invading phase.

$$P_c = \frac{\sigma(\cot \alpha_3 \cos \theta_2 - \sin \theta_2)}{R(\cot \alpha_2 + \cot \alpha_3)} \tag{C30}$$

if only corner 3 has a layer or filled corner of the invading phase.

$$P_c = \frac{\sigma(\cot \alpha_3 \cos \theta_2 - \sin \theta_2)}{R(\cot \alpha_1 + \cot \alpha_3)} \tag{C31}$$

if only corner 3 has a layer or filled corner of the invading phase.

$$P_c = \frac{\sigma}{r_{extreme}} \frac{\cos(\theta_2 + \alpha)}{\cos(\theta_1 + \alpha)}, \quad \theta_2 \leq \pi - \alpha, \tag{C32}$$

$$P_c = \frac{\sigma}{r_{extreme}} \frac{-1}{\cos(\theta_1 + \alpha)}, \quad \theta_2 \geq \pi - \alpha. \tag{C33}$$

Note: In Eqs. (C32) and (C33) α is for the sharpest corner if a layer or filled corner of the invading phase is present in more than one corner.

$$P_c = \frac{\sigma}{R}(\cot \alpha \cos \theta_2 - \sin \theta_2). \tag{C34}$$

Equations (C35)–(C39) are used to compute threshold capillary pressure of layer collapse and formation. Table XIV names which equations are used for layer collapse or formation in different configurations (see Figs. 6 and 7).

TABLE XIII. Threshold capillary pressure for snapoff displacements—water to oil, water to gas, and oil to gas.

Cross section	Contact angle range	Equation(s)	θ_1[a]	θ_2	Comment
Triangular	$\theta_{ij} \leq \pi/2 - \alpha_1$	(C20)–(C31)		θ_{ij}	max P_{cij}
Triangular	$\theta_{ij} \leq \pi - \alpha_1$ and $\theta_{ij} > \pi/2 - \alpha_1$	(C32)	[b]	θ_{ij}	
Triangular	$\theta_{ij} > \pi - \alpha_1$	(C33)	[b]	θ_{ij}	
Square	$\theta_{ij} \leq \pi/4$	(C34)		θ_{ij}	
Square	$\theta_{ij} > \pi/4$ and $\theta_{ij} \leq 3\pi/4$	(C32)	[b]	θ_{ij}	
Square	$\theta_{ij} > 3\pi/4$	(C33)	[b]	θ_{ij}	

[a]Contact angle that interface moved with last time.
[b]It can be either $\pi - \theta_1$ or θ_1 based on the type of AM that θ_1 belongs to. It is the angle that the AM makes with the surface towards the apex of the corner.

TABLE XIV. Threshold capillary pressure for layer collapse and formation events.

Configuration group	Layer	Displacing phase	Equations	σ or σ_1	σ_2	θ or θ_1	θ_2	P_{c1}	P_{c2}	Comment
D and H	oil	water	(C35)	σ_{ow}		θ^h_{ow}				iterative
E and I	gas	water	(C35)	σ_{gw}		θ^h_{gw}				iterative
F and J	oil	water	(C36)–(C38)	σ_{ow}	σ_{go}	θ^h_{ow}	θ^h_{go}		P_{cgo}	iterative
F and J	oil	gas	(C36), (C37), and (C39)	σ_{ow}	σ_{go}	θ^h_{ow}	θ^h_{go}	P_{cow}		iterative
G and K	gas	water	(C36)–(C38)	σ_{gw}	σ_{go}	θ^h_{gw}	$\pi-\theta^h_{go}$		P_{cgo}	iterative
G and K	gas	oil	(C36), (C37), and (C39)	σ_{gw}	σ_{go}	θ^h_{gw}	$\pi-\theta^h_{go}$	P_{cgw}		iterative
H	water	oil	(C36)–(C38)	σ_{ow}	σ_{gw}	$\pi-\theta^h_{ow}$	θ^h_{gw}		P_{cgw}	iterative
H	water	gas	(C36), (C37), and (C39)	σ_{ow}	σ_{gw}	$\pi-\theta^h_{ow}$	θ^h_{gw}	P_{cow}		iterative
I	water	gas	(C36)–(C38)	σ_{gw}	σ_{ow}	$\pi-\theta^h_{gw}$	θ^h_{ow}		P_{cow}	iterative
I	water	oil	(C36), (C37), and (C39)	σ_{gw}	σ_{ow}	$\pi-\theta^h_{gw}$	θ^h_{ow}	P_{cgw}		iterative
J	gas	oil	(C36)–(C38)	σ_{go}	σ_{gw}	θ^h_{go}	$\pi-\theta^h_{gw}$		P_{cgw}	iterative
J	gas	water	(C36), (C37), and (C39)	σ_{go}	σ_{gw}	θ^h_{go}	$\pi-\theta^h_{gw}$	P_{cgo}		iterative
K	oil	gas	(C36)–(C38)	σ_{go}	σ_{ow}	$\pi-\theta^h_{go}$	$\pi-\theta^h_{ow}$		P_{cow}	iterative
K	oil	water	(C36), (C37), and (C39)	σ_{go}	σ_{ow}	$\pi-\theta^h_{go}$	$\pi-\theta^h_{ow}$	P_{cgo}		iterative

$$P_c = \frac{\sigma(3\sin^2\alpha + 4\sin\alpha\cos\theta + \cos^2\theta)}{b[\cos\alpha\sin\alpha(2\sin\alpha + \cos\theta) + \sin^2\alpha\sqrt{4\cos^2\alpha - 3 - \cos^2\theta - 4\sin\alpha\cos\theta}]}. \tag{C35}$$

Note: b is the meniscus-apex distance of the first interface from corner towards the center and θ is the hinging contact angle of the second interface.

$$R_c = \frac{\cos(\theta_2 + \alpha)}{\cos(\theta_1 + \alpha)}, \quad \theta_2 \geqslant \theta_1, \tag{C36}$$

$$R_c = \frac{\cos\theta_2 - \sin\alpha}{\cos\theta_1 - \sin\alpha}, \quad \theta_2 < \theta_1, \tag{C37}$$

$$P_c = \frac{\sigma_1 P_{c2}}{\sigma_2 R_c}, \tag{C38}$$

$$P_c = \frac{\sigma_2 P_{c1} R_c}{\sigma_1}. \tag{C39}$$

[1] M. Honarpour, L. Koederitz, and A. H. Harvey, *Relative Permeability of Petroleum Reservoirs*, 1st ed. (CRC Press, Florida, 1986).
[2] M. J. Oak, L. E. Baker, and D. C. Thomas, JPT, J. Pet. Technol. **42**(8), 1054 (1990).
[3] D. E. Dria, G. A. Pope, and K. Sepehrooni, SPE Reservoir Eng. **8**(2), 143 (1993).
[4] F. A. L. Dullien, *Porous Media: Fluid Transport and Pore Structure*, 2nd ed. (Academic Press, San Diego, 1992).
[5] M. C. Leverett, Trans. Am. Inst. Min., Metall. Pet. Eng. **142**, 152 (1941).
[6] A. T. Corey, C. H. Rathjens, J. H. Henderson, and M. R. J. Wyllie, Trans. Am. Inst. Min., Metall. Pet. Eng. **207**, 349 (1956).
[7] C. S. Land, SPEJ **8**, 149 (1968).
[8] H. L. Stone, JPT, J. Pet. Technol. **22**(2), 214 (1970).
[9] H. L. Stone, J. Can. Pet. Technol. **12**(4), 53 (1973).
[10] J. K. Dietrich and P. L. Bondor, Proceedings of the 51st SPE Annual Technical Conference and Exhibition, New Orleans, LA, 1976.
[11] K. Aziz and A. Settari, *Petroleum Reservoir Simulation*, 1st ed. (Elsevier Applied Science, London, 1979).
[12] F. J. Fayers and J. D. Matthews, SPEJ **24**, 224 (1984).
[13] J. C. Parker, R. J. Lenhard, and T. Kuppusamy, Water Resour. Res. **23**(4), 618 (1987).
[14] L. E. Baker, Proceedings of the SPE/DOE Enhanced Oil Recovery Symposium, Tulsa, OK, 1988, Paper SPE 17369.
[15] F. J. Fayers, SPE Reservoir Eng. **4**, 437 (1989).
[16] M. Delshad and G. A. Pope, Transp. Porous Media **4**(1), 59 (1989).
[17] J. C. Parker and R. J. Lenhard, J. Pet. Sci. Eng. **4**, 57 (1990).
[18] B. F. Marek, K. J. Hartman, and A. E. MacDonald, Proceedings of the SPE Middle East Oil Show held in Bahrain, 1991, Paper SPE 21374.

[19] R. J. Lenhard, J. Contam. Hydrol. **9**(3), 243 (1992).
[20] O. S. Hustad and A. G. Hansen, Proceedings of the Eighth European Symposium on Improved Oil Recovery, Vienna, 15–17 May 1995.
[21] G. R. Jerauld, Proceedings of the 7th ADIPEC, Abu Dhabi, 1996, Paper SPE 36178.
[22] G. R. Jerauld, SPE Reservoir Eng. **12**(1), 66 (1997).
[23] E. F. Balbinski, T. P. Fishlock, S. G. Goodyear, and P. I. R. Jones, Pet. Geosci. **5**(4), 339 (1999).
[24] F. J. Fayers, Proceedings of the SPE/DOE Improved Oil Recovery Symposium, Tulsa, OK, 2000, Paper SPE 59313.
[25] M. J. Blunt, SPEJ **5**(4), 435 (2000).
[26] O. S. Hustad, SPEJ **7**(1), 59 (2002).
[27] M. J. Blunt, SPEJ **2**(4), 494 (1997).
[28] G. G. Pereira, W. V. Pinczewski, D. Y. C. Chan, L. Paterson, and P. E. Øren, Transp. Porous Media **24**(2), 167 (1996).
[29] R. Lenormand, C. Zarcone, and A. Sarr, J. Fluid Mech. **135**(October), 337 (1983).
[30] R. Lenormand and C. Zarcone, Proceedings of the 59th SPE Annual Technical Conference and Exhibition, Houston, TX, 1984, Paper SPE 13264.
[31] J. D. Chen and J. Koplik, J. Colloid Interface Sci. **108**(2), 304 (1985).
[32] I. Chatzis, A. Kantzas, and F. A. L. Dullien, Proceedings of the 63rd SPE Annual Technical Conference and Exhibition, Houston, TX, 1988, Paper SPE 18284.
[33] A. Kantzas, I. Chatzis, and F. A. L. Dullien, Proceedings of the SPE Rocky Mountain Regional Meeting, Casper, WY, 1988, Paper SPE 17506.
[34] A. Kantzas, I. Chatzis, and F. A. L. Dullien, Proceedings of the SPE/DOE Enhanced Oil Recovery Symposium, Tulsa, OK, 1988, Paper SPE 17379.
[35] P. E. Øren and W. V. Pinczewski, SPE Form. Eval. **7**, 70 (1992).
[36] P. E. Øren and W. V. Pinczewski, Proceedings of the 67th SPE Annual Technical Conference and Exhibition, Washington, DC, 1992, Paper SPE 24881.
[37] W. E. Soll, M. A. Celia, and J. L. Wilson, Water Resour. Res. **29**(9), 2963 (1993).
[38] P. E. Øren and W. V. Pinczewski, SPE Form. Eval. **9**(2), 149 (1994).
[39] M. J. Blunt, D. Zhou, and D. H. Fenwick, Transp. Porous Media **20**(1–2), 77 (1995).
[40] P. E. Øren and W. V. Pinczewski, Transp. Porous Media **20**(1–2), 105 (1995).
[41] M. Dong, F. A. L. Dullien, and I. Chatzis, J. Colloid Interface Sci. **172**(1), 21 (1995).
[42] O. Vizika and J. M. Lombard, SPE Reservoir Eng. **11**(1), 54 (1996).
[43] A. A. Keller, M. J. Blunt, and P. V. Roberts, Transp. Porous Media **26**(3), 277 (1997).
[44] P. M. Adler, C. G. Jacquin, and J. A. Quiblier, Int. J. Multiphase Flow **16**(4), 691 (1990).
[45] A. P. Roberts, Phys. Rev. E **56**, 3203 (1997).
[46] C. L. Y. Yeong and S. Torquato, Phys. Rev. E **58**, 224 (1998).
[47] S. Bakke and P. E. Øren, SPEJ **2**(2), 136 (1997).
[48] P. E. Øren, S. Bakke, and O. J. Arntzen, SPEJ **3**(4), 324 (1998).
[49] P. E. Øren and S. Bakke, Transp. Porous Media **46**(2–3), 311 (2002).
[50] J. H. Dunsmuir, S. R. Ferguson, K. L. D'Amico, and J. P. Stokes, Proceedings of the 66th SPE Annual Technical Conference and Exhibition, Dallas, TX, 1991, Paper SPE 22860.
[51] P. Spanne, J. F. Thovert, C. J. Jacquin, W. B. Lindquist, K. W. Jones, and P. M. Adler, Phys. Rev. Lett. **73**(14), 2001 (1994).
[52] A. K. Gunstensen, D. H. Rothman, S. Zaleski, and G. Zanetti, Phys. Rev. A **43**, 4320 (1991).
[53] D. Grunau, S. Chen, and K. Eggert, Phys. Fluids A **5**, 2557 (1993).
[54] B. Ferreol and D. H. Rothman, Transp. Porous Media **20**(1–2), 3 (1995).
[55] F. M. V. Katz and P. J. P. Egberts, Transp. Porous Media **37**(1), 55 (1999).
[56] J. F. Delerue and E. Perrier, Comput. Geosci. **28**(9), 1041 (2002).
[57] I. Fatt, Trans. Am. Inst. Min., Metall. Pet. Eng. **207**, 144 (1956).
[58] I. Fatt, Trans. Am. Inst. Min., Metall. Pet. Eng. **207**, 160 (1956).
[59] I. Fatt, Trans. Am. Inst. Min., Metall. Pet. Eng. **207**, 164 (1956).
[60] M. A. Celia, P. C. Reeves, and L. A. Ferrand, Rev. Geophys. **33**, 1049 (1995).
[61] M. J. Blunt, Curr. Opin. Colloid Interface Sci. **6**(3), 197 (2001).
[62] M. J. Blunt, M. D. Jackson, M. Piri, and P. H. Valvatne, Adv. Water Resour. **25**(8–12), 1069 (2002).
[63] S. Bryant and M. J. Blunt, Phys. Rev. A **46**, 2004 (1992).
[64] S. L. Bryant, D. W. Mellor, and C. A. Cade, AIChE J. **39**(3), 387 (1993).
[65] S. Bryant, P. R. King, and D. W. Mellor, Transp. Porous Media **11**(1), 53 (1993).
[66] L. S. Nilsen, P. E. Øren, S. Bakke, and A. Henriquez, in Proceedings of the European 3-D Reservoir Modelling Conference, Stavanger, Norway, 1996.
[67] T. W. Patzek, SPEJ **6**(2), 144 (2001).
[68] M. Piri and M. J. Blunt, Proceedings of the SPE Annual Technical Conference and Exhibition, San Antonio, TX, 2002, Paper SPE 77726.
[69] P. E. Øren and S. Bakke, J. Pet. Sci. Eng. **39**(3–4), 177 (2003).
[70] P. H. Valvatne and M. J. Blunt, Water Resour. Res. **40**, W07406 (2004).
[71] M. A. Ioannidis and I. Chatzis, J. Colloid Interface Sci. **229**(2), 323 (2000).
[72] C. D. Tsakiroglou and A. C. Payatakes, Adv. Water Resour. **23**(7), 773 (2000).
[73] M. Pillotti, Transp. Porous Media **41**(3), 359 (2000).
[74] Z. R. Liang, P. C. Philippi, C. P. Fernandes, and F. S. Magnani, SPE Reservoir Eval. Eng. **2**, 161 (1999).
[75] R. D. Hazlett, Transp. Porous Media **20**, 21 (1995).
[76] D. A. Coker, S. Torquato, and J. H. Dunsmuir, J. Geophys. Res., [Solid Earth] **101**, 17 497 (1996).
[77] Z. R. Liang, C. P. Fernandes, F. S. Magnani, and P. C. Philippi, J. Pet. Sci. Eng. **21**, 273 (1998).
[78] Z. R. Liang, M. A. Ioannidis, and I. Chatzis, Chem. Eng. Sci. **55**, 5247 (2000).
[79] S. Bekri, K. Xu, F. Yousefian, P. M. Adler, J. Thovert, J. Muller, K. Iden, A. Psyllos, A. K. Stubos, and M. A. Ioannidis, J. Pet. Sci. Eng. **25**, 107 (2000).
[80] J. Quiblier, J. Colloid Interface Sci. **98**, 84 (1984).

[81] P. M. Adler, C. J. Jacquin, and J. F. Thovert, Water Resour. Res. **28**, 1571 (1992).
[82] M. Hilpert and C. T. Miller, Adv. Water Resour. **24**, 243 (2001).
[83] H. J. Vogel and K. Roth, Adv. Water Resour. **24**, 233 (2001).
[84] R. Ehrlich and D. K. Davies, Proceedings of the SPE Gas Technology Symposium, Dallas, TX, 1989, Paper SPE 19054.
[85] G. Mason and N. R. Morrow, J. Colloid Interface Sci. **141**(1), 262 (1991).
[86] M. I. J. van Dijke and K. S. Sorbie, Phys. Rev. E **66**, 046302(2) (2002).
[87] M. I. J. van Dijke, K. S. Sorbie, M. Sohrabi, D. Tehrani, and A. Danesh, SPEJ **9** (1), 57 (2004).
[88] D. H. Fenwick and M. J. Blunt, SPEJ **3**(1), 86 (1998).
[89] D. H. Fenwick and M. J. Blunt, Adv. Water Resour. **21**(2), 121 (1998).
[90] J. K. Larsen, N. Bech, and A. Winter, Proceedings of the SPE/DOE Improved Oil Recovery Symposium, Tulsa, OK, 2000, Paper SPE 59324.
[91] P. A. Goode and T. S. Ramakrishnan, Am. Ind. Hyg. Assoc. J. **39**(7), 1124 (1993).
[92] H. N. Man and X. D. Jing, Transp. Porous Media **41**(3), 263 (2000).
[93] A. W. Adamson and A. P. Gast, *Physical Chemistry of Surfaces* (John Wiley and Sons, Inc., New York, 1997), 6th ed.
[94] D. Zhou and M. J. Blunt, J. Contam. Hydrol. **25**(1), 1 (1997).
[95] F. E. Bartell and H. J. Osterhoff, Ind. Eng. Chem. **19**, 1277 (1927).
[96] M. J. Blunt, J. Colloid Interface Sci. **239**(1), 281 (2001).
[97] M. I. J. van Dijke, K. S. Sorbie, and S. R. McDougall, Adv. Water Resour. **24**(3–4), 365 (2001).
[98] N. R. Morrow, H. T. Lim, and J. S. Ward, SPE Form. Eval. **2**, 89 (1986).
[99] O. Fassi-Fihri, M. Robin, and E. Rosenberg, Proceedings of the 66th SPE Annual Technical Conference and Exhibition, Dallas, TX, 1991, Paper SPE 22596.
[100] A. R. Kovscek, H. Wong, and C. J. Radke, AIChE J. **39**(6), 1072 (1993).
[101] J. S. Buckley, Y. Liu, and S. Monsterleet, SPEJ **3**(1), 54 (1998).
[102] L. W. Lake, *Improved Oil Recovery* (Prentice-Hall, Englewood Cliffs, NJ, 1989).
[103] N. R. Morrow, J. Can. Pet. Technol. **14**(4), 42 (1975).
[104] N. R. Morrow, J. Can. Pet. Technol. **15**(4), 49 (1976).
[105] N. J. Hayden and T. C. Voice, J. Contam. Hydrol. **12**(3), 217 (1993).
[106] M. Dong and I. Chatzis, J. Colloid Interface Sci. **172**(2), 278 (1995).
[107] A. A. Heiba, H. T. Davis, and L. E. Scriven, Proceedings of the SPE/DOE Symposium on Enhanced Oil Recovery, Tulsa, OK, 1984, Paper SPE 12690.
[108] A. A. Heiba, H. T. Davis, and L. E. Scriven, Proceedings of the 58th SPE Annual Technical Conference and Exhibition, San Francisco, CA, 1983, Paper SPE 12172.
[109] A. A. Heiba, M. Sahimi, L. E. Scriven, and H. T. Davis, SPE Reservoir Eng. **7**, 123 (1992).
[110] R. B. Stinchcombe, J. Phys. C **7**, 179 (1974).
[111] W. E. Soll and M. A. Celia, Adv. Water Resour. **16**, 107 (1993).
[112] P. E. Øren, J. Billiotte, and W. V. Pinczewski, Proceedings of the SPE/DOE Symposium in Improved Oil Recovery, Tulsa, OK, 1994, Paper SPE 27814.
[113] P. E. Øren and W. V. Pinczewski, Proceedings of the 6th European IOR Symposium, Stavanger, 1991.
[114] R. Chandler, J. Koplik, K. Lerman, and J. F. Willemsen, J. Fluid Mech. **119**, 249 (1982).
[115] D. Wilkinson and J. F. Willemsen, J. Phys. A **16**, 3365 (1983).
[116] M. J. Oak, Proceedings of the 66th SPE Annual Technical Conference and Exhibition, Dallas, TX, 1991, Paper SPE 22599.
[117] M. J. Oak, Proceedings of the SPE/DOE Seventh Symposium on Enhanced Oil Recovery, Tulsa, OK, 1990, Paper SPE 20183.
[118] L. Paterson, J. Y. Lee, and W. V. Pinczewski, Proceedings of the SPE Annual Technical Conference and Exhibition, San Antonio, TX, 1997, Paper SPE 38882.
[119] L. Paterson, S. Painter, X. Zhang, and W. V. Pinczewski, Proceedings of the SPE Annual Technical Conference and Exhibition, Denver, CO, 1996, Paper SPE 36523.
[120] J. Hoshen and R. Kopelman, Phys. Rev. B **14**, 3438 (1976).
[121] A. S. Grader and D. J. O'Meara, Proceedings of the 63rd SPE Annual Technical Conference and Exhibition, Houston, TX, 1988, Paper SPE 18293.
[122] S. G. Goodyear and P. I. R. Jones, Proceedings of the 7th European IOR Symposium, Moscow, Russia, 1993.
[123] P. Naylor, N. C. Sargent, A. J. Crosbie, A. P. Tilsed, and S. G. Goodyear, Proceedings of the 8th European IOR Symposium, Vienna, Austria, 1995.
[124] A. Sahni, J. Burger, and M. J. Blunt, Proceedings of the SPE/DOE Improved Oil Recovery Symposium, Tulsa, OK, 1998, Paper SPE 39655.
[125] M. C. Leverett and W. B. Lewis, Trans. Am. Inst. Min., Metall. Pet. Eng. **142**(107), 107 (1940).
[126] J. E. Nordtvedt, E. Ebeltoft, J. E. Iversen, A. Sylte, H. Urkedal, K. O. Vatne, and A. T. Watson, Proceedings of the SPE Annual Technical Conference and Exhibition, Denver, CO, 1996, Paper SPE 36683.
[127] V. Mani and K. K. Mohanty, J. Colloid Interface Sci. **187**(1), 45 (1997).
[128] V. Mani and K. K. Mohanty, SPEJ **3**, 238 (1998).
[129] K. K. Mohanty and S. J. Salter, Proceedings of the 57th SPE Annual Fall Technical Conference and Exhibition, New Orleans, LA, 1982, Paper SPE 11018.
[130] C. Laroche, O. Vizika, and F. Kalaydjian, J. Pet. Sci. Eng. **24**(2–4), 155 (1999).
[131] C. Laroche, O. Vizika, and F. Kalaydjian, Proceedings of the SPE Annual Technical Conference and Exhibition, Houston, TX, 1999, Paper SPE 56674.
[132] M. H. Hui and M. J. Blunt, J. Phys. Chem. B **104**(16), 3833 (2000).
[133] T. R. Lerdahl, P. E. Øren, and S. Bakke, Proceedings of the SPE/DOE Symposium in Improved Oil Recovery, Tulsa, OK, 2000, Paper SPE 59311.
[134] M. I. J. van Dijke, K. S. Sorbie, and S. R. McDougall, Proceedings of the SPE/DOE Symposium in Improved Oil Recovery, Tulsa, OK, 2000, Paper SPE 59310.
[135] M. I. J. van Dijke, S. R. McDougall, and K. S. Sorbie, Transp. Porous Media **44**(1), 1 (2001).
[136] M. Sohrabi, G. D. Henderson, D. H. Tehrani, and A. Danesh,

Proceedings of the SPE Annual Technical Conference and Exhibition, Dallas, TX, 2000, Paper SPE 63000.
[137] M. Sohrabi, D. H. Tehrani, A. Danesh, and G. D. Henderson, Proceedings of the SPE Annual Technical Conference and Exhibition, New Orleans, LA, 2001, Paper SPE 71494.
[138] D. Zhou, M. J. Blunt, and F. M. Orr, J. Colloid Interface Sci. **187**(1), 11 (1997).
[139] F. J. M. Kalaydjian, Transp. Porous Media **5**(3), 215 (1990).
[140] R. P. Mayer and R. A. Stowe, J. Colloid Sci. **20**, 893 (1965).
[141] H. M. Princen, J. Colloid Interface Sci. **30**(1), 69 (1969).
[142] H. M. Princen, J. Colloid Interface Sci. **30**(3), 359 (1969).
[143] H. M. Princen, J. Colloid Interface Sci. **34**(2), 171 (1970).
[144] A. Al-Futaisi and T. W. Patzek, Physica A **321**(3–4), 665 (2003).
[145] R. Sedgewick, *Algorithms in C++. Part 5:Graph Algorithms*, 3rd ed. (Addison-Wesley, Boston, 2002).
[146] F. J. M. Kalaydjian, Proceedings of the 67th SPE Annual Technical Conference and Exhibition, Washington, DC, 1992, Paper SPE 24878.
[147] T. C. Ransohoff and C. J. Radke, J. Colloid Interface Sci. **121**(2), 392 (1988).
[148] M. J. Blunt, J. Pet. Sci. Eng. **20**(3–4), 117 (1998).
[149] T. W. Patzek and D. B. Silin, J. Colloid Interface Sci. **236**(2), 295 (2001).
[150] T. C. Ransohoff, P. A. Gauglitz, and C. J. Radke, AIChE J. **33**(5), 753 (1987).
[151] T. W. Patzek and J. G. Kristensen, J. Colloid Interface Sci. **236**(2), 305 (2001).
[152] A. Al-Futaisi and T. W. Patzek, SPEJ **8**(3), 252 (2003).